University of Twente

Bachelor Assignment

Drug targeting inflammatory macrophages in the synovial membrane using VHH coated LNPs

Roy Fakkert (s2611112)

Developmental BioEngineering (DBE)

Supervisor:
Prof. Dr. Marcel Karperien

Daily supervisors:
Dr. B. Zoetebier
Dr. J. Hendriks

Extern committee member:
Dr. Ruchi Bansal

June 29, 2023

UNIVERSITY OF TWENTE. | TECHMED CENTRE | Developmental BioEngineering

Table of contents

Abstract

Synovitis is the inflammation of the synovial membrane and is present in joint diseases like osteoarthritis (OA) and rheumatoid arthritis (RA). This affects more than half of the population above age 65. Macrophages play an important role in the progression of synovitis. Activation of the different types of macrophages is a factor in the severity of OA and RA. Because of this, drugs that can target macrophages could be used to develop therapies that slow down the progression of OA and/or stimulate regeneration. MiRNA has been shown to have an important role in the biological processes of macrophages such as polarization. However, miRNA needs to be protected and transported to the target, because it is degraded fast in the body. A way to encapsulate and transport miRNA is by using ionizable lipid nanoparticles. When these ionizable LNPs are released in the body, they are neutral at physiological pH. If taken up by a cell in an endosome, the low pH causes the LNPs to become cationic, after which they are broken down and can release their content. For targeting specific types of macrophages only, the LNPs need to be coated with biomolecules. A biomolecule gaining significant attention is the VHH, which is an antibody fragment that has almost the same binding characteristics as normal antibodies but is way smaller. So, in this report, LNPs are made that have VHHs conjugated to them. As a proof of concept, the LNPs contain dsDNA and tRNA instead of miRNA. The LNPs are conjugated with TNFα-specific VHHs. Lipid nanoparticles containing ionizable lipid DLin-MC3-DMA are made under low pH conditions, so this ionizable lipid is positively charged to make encapsulation of the negative nucleic acids possible. The LNPs were synthesized using a T-tubing method. The lipid phase, which consists of the different lipids dissolved in ethanol in a certain molar ratio, is mixed with the DNA phase, which consists of DNA dissolved in water. The phospholipid DSPE-PEG-Maleimide that is present in the LNPs makes conjugation of the VHHs via maleimide-thiol chemistry possible. Adding the LNPs containing DSPE-PEG-Maleimide and the VHHs together in different ratios results in different amounts of VHHs on the surfaces of the LNPs. DLS measurements were performed to quantify the size, polydispersity and surface charge of the LNPs. Size and zeta potential measurements were done on LNPs with and without DSPE-PEG-Mal and with different amounts of VHHs per LNP. The results show that the LNPs have a diameter of around 180nm. Zeta potential measurements show a high variety in surface charge in conditions of VHHs with LNPs. SEM is used to show the morphology and structure of the formed LNPs. To quantify whether VHHs are conjugated to the LNPs containing maleimide groups on their surface SDS-PAGE and western blot were performed. Furthermore, fluorescent dyes were used in the LNP composition and attached to the VHHs. Unfortunately, no specific VHH conjugation with LNPs containing DSPE-PEG-Mal was observed. The LNPs and VHHs with fluorescent dyes were also used to show LNP uptake in macrophages in a cell experiment with the RAW 264.7 cell line. This did show signs of LNP uptake by the macrophages, but not for LNPs with VHHs specific. The conclusion is that LNPs are formed, but that the conjugation with VHHs is not yet detected and maybe not even present. Furthermore, it remains to be seen whether VHH-LNP conjugates make effective targeted drug delivery possible. The TNFα-specific VHHs are used for testing conjugation to LNPs and don't target macrophages.

1 Introduction

Synovitis is the inflammation of the synovial membrane and is present in joint diseases like osteoarthritis (OA) and rheumatoid arthritis (RA) [1]. OA and RA are diseases associated with joint pain, synovial fibrosis and osteophyte formation. This affects more than half of the population above age 65 and this group is expected to increase with the ageing of the population [2].

Monocytes and macrophages play an important role in the progression of synovitis in OA and RA. Monocytes are located in the blood and turn into macrophages when they become active in tissue. Activated macrophages can be polarized into M1 and M2 types of macrophages. M1 macrophages are pro-inflammatory, while M2 macrophages are pro-regenerative [3]. Activation of the types of macrophages and the ratio M1/M2 are factors in the severity of OA [4]. Because of this, drugs that can target monocytes and macrophages could be used to develop therapies that slow down the progression of synovitis and stimulate regeneration.

1.1 Monocytes and macrophages

Macrophages can be targeted in many different ways. In the case of slowing down the progression of OA and RA, inflammations of the synovial membrane should be prevented. For this, the intra- and extracellular pathways that activate M1 macrophages can be inhibited. In the case of regeneration of tissue pathways that activate M2 macrophages should be stimulated. The cytokinetic environment in which a monocyte or macrophage is present will determine in which phenotype the polarization occurs. For example, polarization into M1 macrophages is induced by pro-inflammatory cytokines IL-1β, IL-6 and TNFα [5]. Specific targeting of certain monocytes or macrophages is necessary because there are many types having different functions, for example in inflammation regulation. Because of this, the types of monocytes or macrophages and their markers are defined.

1.1.1 Markers for types of monocytes

Three major types of monocytes can be described; classical, non-classical and intermediate monocytes. Monocytes are produced in the bone marrow and released in the blood as classical monocytes, which are also the most commonly found monocyte in the blood. They can differentiate to become non-classical and intermediate monocytes. They are distinguished from each other by their expression of specific surface receptors. The most important surface receptors in monocytes are CD14 and CD16, and their expression levels specify their type. These levels are given in Table 1 [6, 7].

Classical monocytes are determined by a very high expression of CD14 and low expression of CD16, defined as $CD14^{++}CD16^{-}$. They can differentiate into macrophages and play a role in forming inflammations by producing pro-inflammatory cytokines. [6]

Non-classical monocytes are determined by a very high expression of CD14 and high expression of CD16, defined as $CD14^{++}CD16^{+}$. They are associated with wound healing processes and anti-viral responses. Non-classical monocytes do produce pro-inflammatory cytokines, but not as many as classical monocytes do. [6]

Intermediate monocytes are determined by a very high expression of CD14 and low expression of CD16, defined as $CD14^{++}CD16^{-}$. These expression levels are comparable to the expression levels of classical monocytes. However, other highly expressed genes are different. They are specialized in antigen presentation and play an essential role in the progression of HIV infections. The inflammatory role of these monocytes is not clear yet and further research needs to be done. [6]

Additionally, from gene expression analysis in healthy individuals, the expression of other receptor genes was found and was specified per type of monocyte. These genes are also shown in Table 1.

Table 1: *The expression levels of surface receptors CD14 and CD16 per type of monocyte. + is a high expression level, ++ is a very high expression level, − is a low expression level, −− is a very low expression level. In addition, other expressed receptor genes are shown. [7]*

Type of monocyte	**Expression level CD14 marker [7]**	**Expression level CD16 marker [7]**	**Other receptor genes expressed [8–10]**
Classical	++	−	CD(54, 11B, 33, 52L, 1d, 9, 99, 91, 64, 35), CCR(1, 2), CXCR(1, 2, 4), CLEC(4D, 5A), IL13Ra1
Non-classical	++	+	CD(115, 97, 123, 294, 31, 43, 11a, 47) CXC3CR1, P2RX1, Siglec10
Intermediate	++	−	CD(40, 80, 32, 54, 163, 74, 202B, 105), HLA(-ABC, -DR), CCR5, CLEC10a, GFRa2

1.1.2 Markers for types of macrophages

Macrophages are divided into two major types; M1 and M2 macrophages. The M1 phenotype is classified as pro-inflammatory, while the M2 phenotype is classified as pro-regenerative. The M1 macrophages are characterized by high expression of genes such as major histocompatibility complex class II (MHC II), CD80, CD86, and TLR4. Expression of these CD80 and CD86 genes stimulates the production of cytokines, enhancing the inflammatory amplification loop [11]. M2 macrophages are associated with the expression of genes such as CD163 and CD206 [12–14].

A more elaborate list of genes that are expressed in the two types of macrophages that can be used as markers, is given in Table 2. In addition, this Table presents the key transcription factors and secreted chemo- and cytokines that play an important role in fulfilling their function and mostly also in polarization.

Table 2: *Elaborate list of expressed genes in the two types of macrophages.*

Type of macrophage	**Expressed genes/markers on surface [14, 15]**	**Key transcription factors [14, 15]**	**Chemo- and cytokines released [14, 15]**
M1	CD(80, 86), TLR(2, 4), iNOS and MHC II	NF-kB, STAT1, STAT5, IRF3, and IRF5	IFN-γ, IL-(1α, 1β, 6, 12, 23), TNF-α, CXCL(9, 10) and ROS
M2	CD(206, 163, 209), FIZZ1, and Ym1/2	STAT6, IRF4, JMJD3, PPARδ, and PPARγ	IL-10, TGF-β and CCL(1, 17, 18, 22, 24)

1.1.3 Subtypes of macrophages

The M1 and M2 macrophages are further divided into subtypes: M1a, M1b, M2a, M2b, M2c and M2d. These different subtypes differ in markers, function, and secreted chemo- and cytokines. However, distinguishing them is not simple, because of their intertwined induction routes and biological functions. [14]

M1a classical macrophages are activated by IFN-γ and Lipopolysaccharide (LPS) and release IL-1, IL-12, IL-23, TNF-α and reactive oxygen species (ROS). They have high expression of MHC II and IL-1R and stimulate phago- and endocytotic behaviour. It is a bactericidal macrophage active in the early stages after injury and can also serve as an antigen-presenting cell. M1b innate macrophages are activated by endogenous danger signals such as HMGB1, iron, histones/ATP and ligate pattern recognition receptors. These signals can be produced in sterile injuries and stimulate an inflammatory response. Yet, this can also limit epithelial healing and induce tissue damage and dysfunctions. M1b macrophages can ingest apoptotic cells and release IL-1, IL-6 and ROS. [15]

M2a macrophages are activated by IL-4 or IL-13 cytokines and lead to the expression of IL-10, TGF-β, CCL17, CCL18, and CCL22. These macrophages enhance endocytic behaviour, cell growth and tissue repair and are also known as alternatively activated macrophages. M2b macrophages can be activated by the immune complex, Toll-like receptors (TLRs) or IL-1β. They release TNF-α, IL-1β, IL-6, and IL-10, which are both pro- and anti-inflammatory. M2b macrophages regulate the breath and depth of immune and inflammatory responses to for example infections. M2c macrophages are activated by glu-

cocorticoids, IL-10 and TGF-β and release IL-10, TGF-β, CCL16, and CCL18 chemo- and cytokines. They are inactivated or regulatory macrophages and are important in regulating phagocytosis and apoptosis. Together with M2d macrophages matrix synthesis is stimulated [14,15]. M2d macrophages are activated by TLRs and secrete IL-10 and vascular endothelial growth factors (VEGF). These macrophages stimulate angiogenesis and tumour progression [14].

1.2 miRNAs in macrophages

MicroRNAs (miRNAs) are short, non-coding RNA strands, that have an important role in some pathophysiological processes. As a drug for macrophages, they have the advantage over mRNAs because they can influence the behaviour by regulating gene expression [16]. MiRNAs also seem to play a role in the biological functions of macrophages. Some studies determined the expression of miRNAs in the different phenotypes [17]. Zhang et al. [18] determined these expression profiles by first using murine bone marrow-derived macrophages and polarizing them under certain conditions, after which miRNA-microarray and qRT-PCR were performed. Cobos Jimenez et al. [19] used polarized monocytes derived from human peripheral blood mononuclear cells to determine the expression profiles with miRNA-microarray and qRT-PCR. The results from both studies are shown in Table 3, summarizing the miRNA expression profiles in M1 and M2 phenotypes. Other studies analysed individual miRNAs and the phenotype which they stimulate, these are also given in Table 3.

Table 3: *Summary of the expressed miRNAs in M1 and M2 macrophages determined by different studies*

Type of macrophage	**Expressed miRNAs (Zhang et al. [18])**	**Expressed miRNAs (Cobos Jimenez et al. [19])**	**Expressed miRNAs in other studies**
M1	miR-155-5p Let-7f-1-3p miR-146a-5p miR-33a-3p miR-542-5p miR-221-5p miR-221-3p	miR-491-5p miR-652-3p miR-652-5p	miR-21 [20] miR-9 [21] miR-127 [22] miR-155 [23] miR-125b [24]
M2	Let-7f-2-3p Let-7f-5p miR-146a-5p miR-301a-3p miR-33a-5p miR-542-5p miR-221-5p miR-221-3p	miR-200a-3p miR-190a miR-652-5p miR-136-5p miR-125b-5p	miR-21 [25] miR-124 [26] miR-223 [27] miR-34a [28] Let-7c [29,30] miR-132 [31] miR-146a [32] miR-125a-5p [33]

These miRNAs can be used to influence the behaviour of macrophages, for example by stimulating polarization into certain phenotypes by initiating intracellular pathways [16].

1.2.1 MiRNAs stimulating macrophage polarization

Some studies investigated the role of miRNA in the polarization of macrophages in diseases like obesity, cancer and multiple sclerosis. In obesity, overexpression of M2-associated miR-223 [34] and inhibition of M1-associated miR-33 [35] showed to result in positive effects. The overexpression of M1-associated miR-155 [36] and downregulation of M2-associated miR-124 [37] appear to result in the irritation of multiple sclerosis. These and other studies suggest that the miRNAs shown in Table 3 and other macrophage-associated miRNAs could indeed be used to polarize activated macrophages into M1 and M2 phenotypes [17].

1.2.2 Targeting macrophages using miRNA-loaded LNPs

Because miRNAs are degraded in the body fast, they need to be protected to be able to be used as a drug [38]. In addition, the miRNA needs to be transported to the macrophages it has to target.

Nanoparticles have been shown to be potentially useful for this targeted drug delivery. These are nanosized drug-loaded vesicles that can have targeting biomolecules attached to them. Due to their small size, they can pass biological barriers and they can be engineered to have certain characteristics [39]. There are many types of NPs including metallic, organic, inorganic and polymeric nanostructures. Lipid nanoparticles (LNPs) are organic NPs that are already extensively used as targeted drug-carrier systems. They are often biodegradable and biocompatible, making them non-toxic [40].

1.3 Lipid nanoparticles (LNPs)

Lipid nanoparticles (LNPs) have been investigated for decades as drug carriers and can be used for specific targeting of drugs. These LNPs can be utilised to carry molecules and nucleic acids like DNA and miRNA because of their biodegradability and encapsulation efficiency. There are multiple classes of LNPs that are distinguishable in the way they are structured and the way they carry drugs. These classes are liposomes, solid lipid nanoparticles (SLNs), nanostructured lipid carriers (NLCs) and lipid-drug conjugates (LDCs) [41, 42].
The LNP classes are explained below and a summary of is presented in Table 4.

1.3.1 Liposomes

Liposomes are the first discovered LNPs and are already in use for a long time. They are spherical vesicles that consist of an amphipathic phospholipid bilayered shell and a core that is an aqueous solution. This structure makes it possible to load hydrophilic and hydrophobic molecules; hydrophilic molecules can be encapsulated in the aqueous core, while hydrophobic molecules can be encapsulated in the lipid bilayer [41, 43]. The first nano-drug approved by the FDA is a liposome-based drug named Doxil. This is a doxorubicin-loaded PEGylated liposome that can be used for targeting solid tumours [41, 44]. The lipid bilayered shell is usually made from phospholipids or synthetic amphiphiles that incorporate sterols to control its permeability. The most commonly used preparation method is thin-film hydration in which lipid components are dissolved together with the drug. Then evaporation followed by rehydration of the film in an aqueous solvent will eventually form the liposome [43, 44]. Other preparation methods are given in Table 4. A liposome can be used for drug delivery by releasing its content in a cell via degradation of its lipid bilayer, fusion of its membrane with the cell membrane and by receptor-mediated endocytosis [43]. Some different subtypes of liposomes can be described.

Stealth or PEGylated liposomes are liposomes that have polymer strands attached to them to avoid detection by the immune system. PEG is the most commonly used and it is linked by the incubation of a reactive derivative of PEG with the target liposome. PEGylation does however affect the physiochemical properties of the liposome, like making it bigger. This causes the circulation time to be longer due to slower renal clearance [43, 44]. Therefore, PEGylated liposomes can slowly accumulate into tumours because of their leaky character. An example of a PEGylated liposome is Doxil [43].

Non-PEGylated liposomes (NPLs) can have the benefits of a PEGylated liposome, while not having the side-effects. For example, NPL Doxorubicin (NPLD) compared to Doxil reduces dose-limited toxicity like the hand-foot syndrome (HFS). This difference is possible due to its special composition which gives it its desired physiochemical properties. They do however have a shorter circulation time than PEGylated liposomes. An example of an NPLD is Myocet. [43]

DepoFoam liposome is a patented technology by Pacira Pharmaceuticals, Inc., Parsippany, NJ, USA. DepoFoam liposomes have extended-release drug delivery due to their multivesicular structure. The liposome is structured with multiple internal aqueous chambers containing spheroids with drugs. This structure causes the outer chambers to release their drugs first and the inner chamber last. This can happen over a time period ranging from around 1 to 30 days. Examples of DepoFoam liposomes are Depocyt, DepoDur and Exparel. [43]

Lysolipid Thermally Sensitive Liposomes (LTSLs) are, as their name suggests, temperature sensi-

tive. Lipids used for this application typically have a transition temperature between 40 and 45 °C. LTSLs are used to release encapsulated drugs at local tissue. This can be done by elevating this tissue to temperatures around 42 °C with radiofrequency ablation. At this temperature, the lipids become more permeable making it possible to release the drugs. An example is ThermoDox, which has 25 times higher drug concentration at the targeted area than free doxorubicin (DOX) [43]. Also, pH-sensitive and redox potential-sensitive liposomes exist [44].

1.3.2 Solid lipid nanoparticles (SLNs)

Solid lipid nanoparticles (SLNs) are spheres made of a solid fully crystallized lipid matrix. They are drug-incorporated with emulsifiers and typically have lipids with higher melting temperature than body temperature such as triglycerides, fatty acids, and waxes. Due to their solid structure, SLNs are stable, have good drug protection and have tuneable properties. The choice of lipid and surfactant components can improve their quality and physiochemical properties. Their disadvantage is low drug-carrying capacity and poor long-term drug retention. Their low drug-carrying capacity is caused by close packing due to crystallization, especially in highly purified lipids. Different subtypes of SLNs can be distinguished, which are different in preparation method and drug encapsulation [41]. An SLN can be used as a drug delivery system by using cationic or ionizable lipid components. These lipid components can encapsulate negatively charged molecules like miRNA and release it when entering a cell via endocytosis [45].

The solid solution model describes an equal spread of drugs over the whole SLN matrix [45, 46]. This can be accomplished with cold homogenization, in which the drug and lipids are evenly spread in solution without a surfactant. After solidification, a homogeneous matrix is formed and if put in a surfactant, the drugs are maintained in the core [46].

The drug-enriched shell model describes a high concentration of drug molecules in the shell of the SLN [45, 46]. This can be accomplished with thermal homogenization, in which a solid lipid core is created at the recrystallization temperature of cooling and the drug is then concentrated in the liquid lipid shell of the SLN due to dispersion temperature reduction [46].

The drug-enriched core model describes a high concentration of drug molecules in the shell of the SLN [45, 46]. This can be done by dissipating drug molecules in melting liquid before cooling, which causes supersaturation of the drug dissolved in the lipid. Then cooling leads to recrystallization of the shell surrounding the drug-lipid solution [46].

1.3.3 Nanostructured lipid carriers (NLCs)

Nanostructured lipid carriers (NLCs) are actually the second generation of SLNs. These LNPs have a solid lipid composition incorporated with liquid lipid components making them less crystalline. This less-ordered structure gives NLCs a higher drug-carrying capacity than SLNs. Although their improved properties with respect to SLNs, they are associated with having low stability and causing cytotoxic effects. The NLCs can also be divided into three subtypes. [41, 46, 47]

The amorphous NLC is, as its name suggests, not crystalline but homogeneous amorphous. This is caused by the adoption of lipids like hydroxyl octacosanol, isopropyl myristate, and hydroxyl stearate, which makes crystallization impossible. [47]

The imperfect NLC consists of disordered crystals with amorphous regions. These regions are made by using small amounts of liquid lipids in a solid lipid matrix with varying chain lengths. The amorphous regions can encapsulate drugs, which increases drug-loading capacity but lowers encapsulation efficiency. [47]

The multiple NLC has high liquid lipid content. The liquid lipids are dispersed into a solid lipid

matrix to induce phase separation. This forms regions in the solid matrix of drug molecules surrounded by liquid lipid components. The advantages are high encapsulation efficiency and controlled drug release. [47]

1.3.4 Lipid-drug conjugates (LDCs)

Lipid-drug conjugates (LDCs) are created to increase drug-loading capacity. Generally, LDCs are produced by first making a lipid-drug conjugate bulk by covalent or non-covalent linking via salt formation. Then this LDC bulk is processed in an aqueous surfactant solution to form nanoparticle-like structures [42, 48]. The LDC bulk is often made by linking the drug molecules to fatty acids, glycerides, waxes and phospholipids via amide, ether and ester bonds. This LDC bulk can then be used to form for example SLN- or NLC-like structures, resulting in LDC-NPs. This can reduce the particle size because drugs don't need to be encapsulated because they are already attached to the lipid consituents [42,48,49]. The preparation methods shown in Table 4 for SLNs and NLCs can often also be used to make these LDC-NPs.

Table 4: *Summary of LNPs types with their structure, preparation methods, advantages, subtypes and some examples [41–49]*

LNP type	Structure	Preparation methods	Advantages	Subtypes	Examples
Liposomes [41, 43, 44]	Lipid bilayered shell and a core with aqueous solution	Thin-film hydration Reverse-phase evaporation Freeze-drying Ethanol injection	Well established Control kinetics/dynamics Improved bioavailability Limited toxicity	Stealth (PEGylated) Non-PEGylated DepoFoam Lysolipid Thermally Sensitive	Doxil Myocet, Depocyt ThermoDox
Solid LNPs (SLNs) [41, 45, 46]	Solid fully crystallized lipid matrix	Homogenization Ultrasonication Micro emulsification Solvent emulsification/ evaporation	Stable Good drug protection Tuneable properties	Solid solution Drug-enriched shell Drug-enriched core	Triglycerides Fatty acids Waxes
Nanostructured lipid carriers (NLCs) [41, 46, 47]	Solid lipid components with liquid lipid components	Homogenization Ultrasonication Micro emulsification Solvent emulsification/ evaporation	Drug-carrying capacity Controlled drug release Tuneable properties	Amorphous Imperfect Multiple	Triglycerides Fatty acids Waxes with oils
Lipid-drug conjugates (LDCs) [42, 48, 49]	Making bulk by linking drug to lipids, then forming SLNs or NLCs	Conjugation via: Ether bonding Ester bonding Amide bonding	Same as SLNs and NLCs but higher drug-carrying capacity	LDC-SLNs LDC-NLC	Fatty acids Glycerides Waxes Phospholipids

In conclusion, a wide variety of LNPs can be used as carriers for drug molecules like miRNA by protecting and transporting them. However, for specific targeting of for example M1 macrophages, LNPs need biomolecules. These biomolecules can be attached to the LNPs surface to form a drug carrier that can be put to use for targeting macrophages via their marker receptors.

1.4 Biomolecules for targeting receptors

If the binding of an LNP to a cell marker via a biomolecule takes place the particles can be taken up by a cell, for example by endocytosis. A drug inside the nanoparticle can then be released into the targeted cell. Possible biomolecules that can be conjugated to the surface of lipid nanoparticles or other biomaterials are peptides, polysaccharides, aptamers, antibodies and antibody fragments [39,50].

1.4.1 Peptides

Peptides are biomolecules that can be used as targeting ligands for receptors. The advantages of peptides are their stability, small size and straightforward conjugation to NPs, but they are degraded fast in the body. The most commonly used peptide is arginylglycylaspartic acid (RGD). This peptide binds to integrins on the surface of cells. These integrins are overexpressed in vascular endothelial cells, so RGD peptides are often used to target cancerous cells. [50]

RGD and some other examples of peptides that can be used to target receptors are given in Table 5.

Table 5: *Peptides that can be used for targeting receptors*

Peptide	**Base sequence**	**Target**
RGD [50]	Arg-Gly-Asp	Integrins
NGR [51]	Asn-Gly-Arg	Tumor (CD13)
BBN(7-13) [52]	Gly-His-Leu-Met-NH2	Tumor (BBN)
RP-182 [53]	Lys-Phe-Arg-Lys-Ala--Phe-Lys-Arg-Phe-Phe	M2 macrophage (CD206)

Some peptides shown in Table 5 are used for targeting cancerous cells. These peptides are recognized by receptors on cancerous cells, to which drug delivery could then be possible [54]. Lastly, the RP-182 peptide is found to bind to receptor CD206. Some studies show that this peptide can therefore be used to target M2 macrophages. However, RP-182 can also bind to RelB and CD47 receptors, which means that it is not just specific to M2 macrophages [53].

1.4.2 Polysaccharides

Polysaccharides are biomolecules built up from monosaccharide units that are linked with glycosidic bonds. They are natural polymers, are stable and have a specific affinity towards receptors. They are structurally and chemically diverse and have functional groups that support stability, encapsulation and specific targeting. Polysaccharides with functional groups can also be used for making NPs and the conjugation between NPs and other ligands. [55]

1.4.3 Aptamers

Aptamers are biomolecules that consist of single-stranded DNA (ssDNA) or RNA (ssRNA). Their nucleotide sequence and unique tertiary structure enable them to bind specifically to their target. Aptamers are selected by the process of Systematic Evolution of Ligands by Exponential Enrichment (SELEX) and the aptamer structure can be produced relatively easy, fast and cheap [56]. SELEX is the incubation of a random collection of ssDNA and ssRNA strands with a specific target. Some ssDNAs and/or ssRNAs will bind, these sequences are detached and amplified using PCR. These amplified strands form aptamers that have a high affinity towards the target molecule. A special type is whole-cell SELEX, which is performing SELEX with whole cells. After multiple rounds, a set of aptamers is obtained that can target multiple receptors. This can for example be used for targeting cancerous cells [57]. Some examples of aptamers that can be used for targeting are shown in Table 6.

Table 6: *Aptamers that can be used for targeting receptors*

Aptamer	**Target**	**Affected cells**
Apt-αvβ3 [58]	αvβ3 integrin	Cancerous
VEap121 [59]	VEGF	Cancerous
AIR-3 [60]	IL-6R	Immune
Aptamer A2 [61]	Specific receptor not found	M0- and M2-macrophages

The study of Sylvestre et al. [61] identified aptamer A2 that binds to M0 and M2 macrophages using whole-cell SELEX. Identifying an aptamer with affinity to M2 macrophages only failed, probably due to high overlap in receptors with M0 macrophages. Also, attempts to identify the specific receptor to which the aptamer binds were unsuccessful.

1.4.4 Antibodies and antibody fragments

Antibodies or immunoglobulins (Igs) are large glycoproteins and can be utilised as biological ligands to target receptors or antigens. These biomolecules are tens of kilodaltons in size which is relatively big. This large size limits the surface density of these targeting ligands on NPs. However, due to their

bigger size, they have very specific binding properties. There are four types of immunoglobulins, of which IgG is the most dominant one in humans. IgGs consist of two identical light protein chains and two identical heavy chains forming a 'Y' shape, shown on the left in figure 1. The N-termini of both the light and heavy chains form the binding sites of the IgGs, these are the variable regions. The other termini of the heavy chains form the constant region. [62]

Antibody fragments can also be used for specific targeting of receptors. Antibody fragments are parts of antibody domains. The fragments always include the variable domain, so specific binding is still possible. A major advantage compared to whole antibodies is a higher possible surface density due to their much smaller size. This makes the nanoparticles more sensitive for binding [62]. A single-domain antibody fragment that is often used nowadays is the Variable heavy domain of the heavy chain only antibody (VHH).

1.4.4.1 Variable heavy domain of the heavy chain only antibodies (VHHs)

Variable heavy domain of the heavy chain only antibodies (VHHs) are a single-domain antibody fragment, illustrated on the right in Figure 1. A VHH is comparable to the variable part of the heavy chain in IgGs. However, the VHHs are not derived from human IgGs because pairing of the light and heavy chain of the variable domain is needed for binding to a target. [63]

Whereas with antibodies in camelids (for example llamas), this domain pairing is not present. These antibodies are heavy chain antibodies, illustrated in the middle of figure 1, and have no light chains. This makes the VHHs around 10 times smaller in size than a normal human IgG. Specific binding is still possible with only the heavy variable domain, the fragment of this domain essentially is a VHH. Production of specific VHHs is mostly done in microorganisms such as *E. coli*, which makes it fast, easy and relatively cheap. VHHs are relatively stable in extreme pH conditions and at high temperatures. A disadvantage is their short half-life due to their small size. [63]

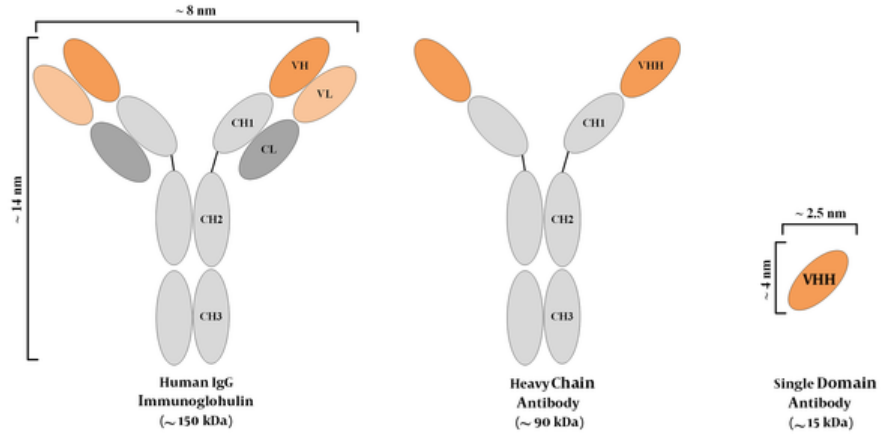

Figure 1: *A simplified representation of an IgG molecule, a heavy chain antibody, and a VHH. The variable domains are shown in orange and the constant domains are shown in grey [64].*

For the biomolecules to be put to use as targeting ligands on LNPs, they need to be attached to the LNP surface. This is done with conjugation chemistry via interactions between functional groups on biomolecules and LNPs to form NP-biomolecule conjugates. This makes the short half-life also less of a problem, because of the increase in size.

1.5 Nanoparticle-biomolecule conjugation chemistry

There are many ways to conjugate make NP-biomolecule conjugates. These conjugates can be used for drug-targeting specific receptors and can be formed with most LNPs described in Section 1.3 and biomolecules presented in Section 1.4. Biomolecules can be attached to nanoparticles or other surfaces via covalent and non-covalent interactions/binding [65, 66]. The conjugation methods are explained below and a schematic overview is given in Figure 2.

1.5.1 Non-covalent binding

NP-biomolecule conjugation via non-covalent typically gives weaker binding than covalent binding. On the other hand, this weaker binding does make it possible for more fragile biomolecules to conjugate to a nanoparticle or surface [65–68]. Some non-covalent interactions are explained below.

1.5.1.1 Electrostatic and hydrophobic interactions

Electrostatic interactions are the adsorption of a biomolecule to a nanoparticle by an opposite charge. For example, a cationic liposome can attract anionic biomolecules such as some peptides. Hydrophobic interactions are possible between hydrophobic nanoparticles or surfaces and hydrophobic biomolecules. These interactions essentially coat the nanoparticle surface with the targeting ligands. An advantage is that the strength of the interaction can be controlled by the choice of nanoparticles and biomolecules. However, strong interactions can for example cause conformational changes in the biomolecule which affects bioactivity, even denaturation is possible. [66–69]

1.5.1.2 Streptavidin-biotin binding

Streptavidin-biotin is a secondary link and is one of the strongest non-covalent biological interactions known [70]. For this interaction, the biomolecule needs to be biotinylated and the nanoparticle surface needs to be streptavidin functionalized. The functionalization with streptavidin or biotin is not always directly possible and sometimes linker molecules are added (for example PEG) or covalent binding methods like the ones explained below are used [67, 68, 71].

1.5.2 Covalent binding

Covalent binding is very strong and stable compared to non-covalent binding [65, 66]. Some covalent binding methods are explained below. Often NPs and biomolecules are attached via bifunctional linkers such as PEG. Linkers can give a NP surface a functional group. PEG gives the surface carboxylic terminated groups suitable for covalent binding [66, 68].

1.5.2.1 Chemisorption

Chemisorption is the chemical adsorption between a surface and an adsorbate in which covalent bonds are formed. An example is the reaction between thiol groups of cysteine residues in biomolecules and functional groups on nanoparticles forming a covalent bond. Most peptides and proteins have cysteine residues with free thiol groups that are able to interact. Sometimes a linker molecule with a thiol group is used instead of the free thiol groups on the biomolecule. The superior nanoparticle surface for chemisorption is gold. Noble metals are highly reactive toward thiol groups. [68]

1.5.2.2 Carbodiimide (EDC/NHS) conjugation

A condensation reaction to form an amide bond is possible between a primary amine in the biomolecule and carboxylic groups on the nanoparticle surface [66]. Generally, peptides and proteins have primary amines in the side chain of lysine residues and the N-terminus. If carboxylic groups on the surface of nanoparticles are not present, bifunctional linkers such as PEG can be added [66, 68]. If the reaction needs to take place in an aqueous environment EDC/NHC crosslinking is often used. EDC is a water-soluble carbodiimide that can form an intermediate compound with the carboxylic component. This intermediate compound is reactive to the amines on the other component and the amide bond can be formed. During this reaction, NHS or sulfo-NHS is often used to increase the EDC-coupling efficiency. This makes the intermediate compound more stable and prevents crosslinking of the biomolecule. The biomolecule can however undergo conformational changes which decreases bioactivity. The orientation of the biomolecule with respect to the nanoparticle depends on which primary amine the carbodiimide is bound to. This can be very non-specific if the biomolecule has multiple lysine residues [66, 67, 71].

1.5.2.3 Maleimide-thiol conjugation

Maleimide-thiol conjugation is possible between the thiol groups in biomolecules and the maleimides attached to the nanoparticle surface. Peptides and proteins have free thiol groups in their cysteine

residues that react with the maleimide attached to the nanoparticle surface, with or without a linker molecule [66, 70, 71]. The reaction between a thiol and a maleimide is a Michael Addition reaction, in which the maleimide has an unsaturated carbonyl group. Other molecules with unsaturated carbonyl groups like acrylates can also be used, but maleimide is most commonly used because it is the most reactive [71]. Sometimes a linker is added to the biomolecule to increase coupling efficiency and reduce unwanted interactions to the nanoparticle surface.

1.5.2.4 Click chemistry

Click chemistry describes a group of strong linking reactions that are easy, have high yield and can be used for the conjugation of many structures. Four major classifications are identified and explained. [66, 72–74]

Cycloaddition is the most commonly used click chemistry and subtypes are copper-catalyzed cycloaddition of azides and terminal alkynes (CuAAC), copper-free cycloaddition strain-promoted alkyne and azide (SPAAC) and Diels-Alder cycloaddition. For CuAAC and SPAAC, the nanoparticle surface needs to be functionalized with azide groups and the biomolecules need to be functionalized with alkyne groups. In CuAAC a copper catalyst is added and triazole-conjugation can take place. In SPAAC the alkyne group is strain-promoted (cyclic) and triazole-conjugation is possible without a copper catalyst. [73, 75]
Nucleophilic ring-opening reactions are openings of strained heterocyclic electrophiles like epoxides and aziridines that are attached to the surface of the nanoparticle, after which they can conjugate with amines on the biomolecule [72, 74].
Carbonyl of non-aldol type chemistry includes the formation of ureas, oximes, hydrazones and aromatic heterocycles [72, 74].
Addition to carbon-carbon multiple bonds often includes Michael addition reactions and oxidation reactions such as epoxidation and aziridination [72, 74].

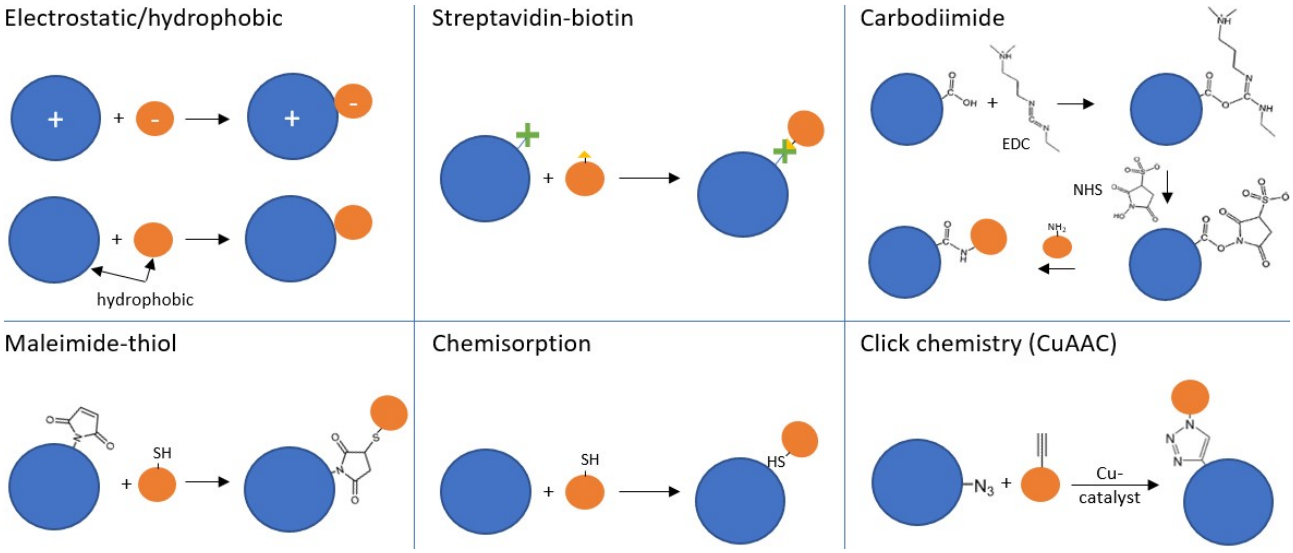

Figure 2: *Schematic overview of methods for the conjugation of biomolecules to nanoparticles. The nanoparticles are illustrated in blue and the biomolecules in orange*

1.6 Encapsulation of miRNA in LNPs with targeting ligands

Delivering miRNA to specific cells can be done by encapsulating the miRNA in LNPs with targeting biomolecules [41]. This is possible with most LNPs explained in Section 1.3 and biomolecules explained in Section 1.4. If the binding of an LNP to a cell receptor via a biomolecule takes place, the particles can be absorbed into the cell through processes like endocytosis, after which the miRNA can then be released [76]. For encapsulation, cationic lipids could be used to complex with the negatively charged miRNA. However, LNPs containing cationic lipids can be cytotoxic because of electrostatic disruption of the negatively charged cell membrane. To solve this problem, ionizable lipids can be used [41, 76].

1.6.1 Ionizable lipids

Ionizable cationic lipids are lipids that have a neutral charge at physiological pH and a positive charge at lower pH. By encapsulating miRNA with LNPs containing these ionizable lipids, the release of miRNA into the targeted cells' cytosol is possible without cytotoxic effects. Due to the neutral charge at physiological pH, the LNPs can pass through the body without a cytotoxic effect to search for cells it can target. If the LNP finds and enters the targeted cell via endocytosis, it comes in contact with a more acidic environment of the endosome. The lower pH causes the ionizable lipid to become positively charged and interact with endogenous anionic lipids. This results in disruption of the endosome, after which the miRNA can be released in the cytoplasm. [41, 76, 77]

These LNPs have more lipid components than just ionizable cationic lipids and together form an SLN-like structure. Phospholipids serve as helper lipids, cholesterol helps with cell entry and PEGylated lipids serve as a coating that improves stability and prevents aggregation [76, 77]. By choosing part of the phospholipids to have functional groups, a targeting biomolecule could be attached by using conjugation chemistry methods explained in Section 1.5 [77]. The making of such an ionizable LNP as a miRNA carrier with targeting ligands is explained below.

1.6.2 Making an ionizable LNP as miRNA carrier

To make these solid ionizable LNPs that encapsulate miRNA, two mixtures need to be made. The lipid mixture consists of the lipid components described above in a certain molar together with ethanol. The aqueous mixture consists of miRNA together with a buffer with a low pH, to make the ionizable lipids cationic. Then both mixtures can be mixed to form a total formulation. This can be done in two ways; using a T-tube or microfluidic-based mixing [41, 77, 78]. Using a T-tube is a more manual approach, while with microfluidic-based mixing the use of automated devices like a NanoAssemblr Benchtop system is possible.

This NanoAssemblr Benchtop system uses a microfluidics chip with a staggered herringbone mixer. With this system, the flow rate ratio between the two mixtures (mostly around 3:1) can be adjusted and relatively monodisperse LNPs should come out [79]. By using the microfluidics chip, mixing is also conducted better. The T-tube (or Y-tube) method can be used if a microfluidic-based mixing system is not available. This is essentially just pumping the two mixtures through the inlets of a T-tube with a certain flow rate ratio between the two. This ratio is different for each set-up and should be adjusted to give good results. The outlet of the T-tube is attached to a tube to give some more space for mixing. This less precise method can result in more polydisperse LNPs. Though, this method does have the possibility to control flow rates using syringes that are automatically actuated. This will in result less polydisperse LNPs than just mixing the lipid and aqueous mixture without control over flow rate.

After mixing the lipid and aqueous mixture, the resultant with LNPs is purified by dialyzing to remove the ethanol and unencapsulated miRNA. The formed LNPs can then be characterized by for example doing DLS measurements to determine the hydrodynamic size, zeta potential and polydispersity index (PDI) [79].

1.7 Aim of this study

The future aim is to target M1 macrophages using CD80-specific VHHs as targeting ligands on the LNPs containing miRNA. VHHs are used because of their high stability and robustness, while still having a strong binding affinity towards their target [63]. LNPs are a suitable choice because of their low immunogenicity, biodegradability and high payload capabilities of nucleic acids [41]. In addition, the use of ionizable lipids makes them controllable under different pH conditions [45]. MiRNAs are used because they have been shown to regulate certain biological processes in macrophages, such as polarization [16]. Additionally, they are efficiently encapsulated by ionizable LNPs.

In this study, the aim is to make LNPs that could be used for specific targeting with VHHs. As a proof of concept, TNFα-specific VHHs are used because their behaviour in terms of conjugation to surfaces like polymeric surfaces is already well known. Additionally, the LNPs are loaded with dsDNA and tRNA instead of miRNA. LNPs will be made using the T-tube method and contain an ionizable lipid (DLin-MC3-DMA), phospholipids (DSPC and DSPE-PEG-Mal), cholesterol and a PEG-lipid (PEG-DMG). Then the TNFα-specific VHHs are attached to the LNP surface by using maleimide thiol conjugation. A simplified schematic representation of the expected structure of the LNPs that will be formed is shown in Figure 3.

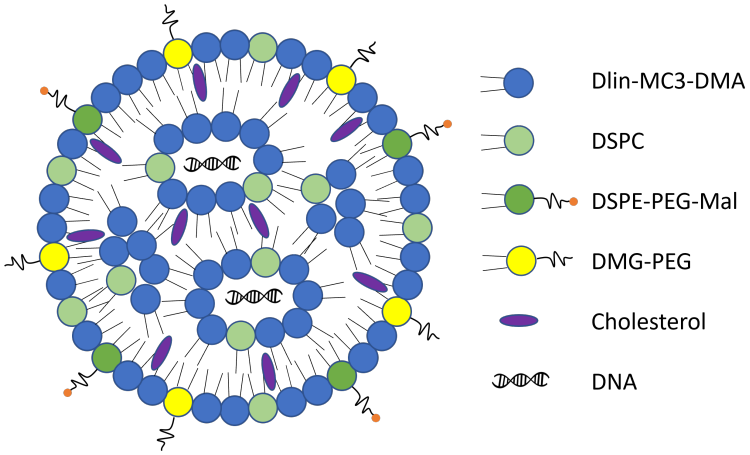

Figure 3: *A simplified schematic representation of the expected structure of the LNPs that will be formed.*

The ionizable lipid that is used is Dlin-MC3-DMA, which has a pKa value of 6.44. This means that below pH 6.44 it has a positive charge and above this pH it has a neutral charge. In the process of making the LNPs, ionizable Dlin-MC3-DMA should be positively charged to attract the negatively charged miRNA.

The PEGylated lipid that is used is DMG-PEG, which is a synthetic lipid and is the PEGylated form of myristoyl diglycerol. It is also used in the Moderna COVID-19 vaccine. Phospholipids that can be used are DSPC and DSPE-PEG-Mal. DSPC is a phospholipid present in cell membranes and is also used in Moderna and Pfizer COVID-19 vaccines. DSPE-PEG-Mal can be used as a conjugation lipid. This phospholipid has a maleimide group that makes maleimide-thiol conjugation possible.

The TNFα-specific VHHs in this study are not conjugated via their own cysteine groups. These VHHs are attached to a Glycerine-Serine 10 peptide linker with a free cysteine on the other end. The Glycerine-Serine 10 peptide linker has peptide sequence $(\text{Gly-Gly-Gly-Gly-Ser})_2$. The free cysteine group is able to conjugate with the maleimide groups from DSPE-PEG-Mal. Adding the linker is done so that the binding affinity of the VHH to its target is not affected by the LNP surface. This also has been shown to improve the coupling efficiency of VHHs to polymers in previous works, which might be the case for coupling to lipids as well.

After LNP synthesis and conjugation of the VHHs, the LNPs and LNP-VHH conjugates are characterized by Dynamic Light Scattering (DLS) and Scanning Electron Microscopy (SEM). SDS-PAGE and western blot are performed, to quantify the binding of the VHHs to the LNPs. Furthermore, fluorescent labelling of the LNPs and VHHs is used to confirm whether DSPE-PEG-Mal is present and reactive on the LNP surface and whether VHHs are conjugated to the LNPs. Lastly, LNPs are incubated with RAW 264.7 macrophages to determine whether the macrophages take up the LNPs.

2 Materials and methods

2.1 Materials

Cholesterol, DSPE-PEG(2000)-Mal, DSPE-PEG(2000)-N-Cy5.5 and DMG-PEG(2000) were purchased from Sigma Aldrich. Dlin-MC3-DMA was purchased from BLDpharm and DSPC from Avanti Polar Lipids. All lipids were prepared in a 10mM ethanol stock and stored at -20 °C until use. The dsDNA that was used is Lambda DNA Standard from a QuantiFluor dsDNA Sample Kit bought at Sigma Aldrich. The tRNA that is used is Invitrogen Yeast tRNA from ThermoFischer. The TNFα-specific VHH used containing a polypeptide linker is biomolecule Q65E5-GS10 (17.8 kDa). The dye that was attached to the targeting biomolecule is a Fluorescein isothiocyanate-N-Hydroxysuccinimide (FITC-NHS) dye. The Cys-dye that is conjugated to the maleimide groups on the LNP surface is a Cys-PEG3-FITC dye. The macrophages used in the cell experiment are from the 264.7 cell line in passage P16.

2.2 T-tube LNP synthesis

First, the lipid mixture was made by mixing specific volumes of ionizable lipid (Dlin-MC3-DMA), phospholipids (DSPC and DSPE-PEG-Mal), cholesterol and a PEG-lipid (PEG-DMG) in a molar ratio of 50/38.5/10/1.5 (mol%), respectively. This mixture had a final lipid concentration of 10 mM. For making LNPs without functionality, only DSPC and no DSPE-PEG-Mal were added. For making LNPs with functional maleimides, the molar ratio between DSPC and DSPE-PEG-Mal was set to 9:1 (mol/mol), respectively. For locating LNPs with a fluorescent Cy5.5 dye in further experiments, 0.2 mol% of DSPE-PEG-N-Cy5.5 was added to the lipid mixture. Secondly, an aqueous mixture is made by diluting the dsDNA or tRNA stock solution in acetate buffer (pH 4), so that the final formulation has an ionizable lipid 10:1 dsDNA/tRNA (wt/wt) ratio. Then both mixtures are mixed using the T-tube (or Y-tube) method. For this method, two syringes were connected to the inlets of a Y-joint using 1mm diameter tubing and some connectors. Tubing was also connected to the outlet to allow some mixing eventually ending up in an Eppendorf tube. This tube was kinked several times creating a turbulent flow that helps with mixing. The two syringes were used to combine both mixtures in a 3:1 aqueous:lipid flow rate ratio (v/v) at a total constant 4 mL/min flow rate. The resultant in the Eppendorf tube is then purified by dialysis with a 3 kDa MWCO filtration membrane in excess MilliQ water. This removed ethanol, resulting in a solution of the LNPs in MilliQ water.

2.3 Labelling VHHs with a FITC-NHS dye

Before the conjugation of VHHs to the LNPs, part of the VHHs was labelled with a FITC-NHS dye by adding a 5 times molar excess of the dye in a 100 mM bicarbonate buffer (pH 8.2) to the VHHs in PBS. After 2 hours of incubation at 4 °C, the free dye was removed by washing the sample 5 times using spin filtration at 14000 rpm for 20 minutes, until the filtrate was colourless. For recovery of the FITC-labelled VHHs, the spin filters were spun upside down for 2 minutes at 1000 rpm.

2.4 Conjugation of VHHs and Cys-PEG3-FITC to LNPs

First, the VHHs and labelled VHHs were reduced to break disulfide bridges in VHH dimers. This was done by adding an excess of TCEP to the VHHs and labelled VHHs in PBS and then incubating them for 1 hour at 37 °C. For conjugation, the VHHs and FITC-labelled VHHs were added to the LNPs with and without DSPE-PEG-Mal in different amounts per LNP, to produce LNP-VHH conjugates in solution. These proportions are calculated from the hydrodynamic size obtained from DLS. According to these calculations, a VHH stock:LNP solution (v/v) ratio of around $1:2*10^6$ should result in 1 VHH per LNP. After adding the VHHs to the LNPs, the mixtures were then stirred overnight at 4 °C.

To be able to show whether DSPE-PEG-Mal is reactive on the LNP surface by using fluorescence, a Cys-PEG3-FITC dye that binds to maleimide was conjugated in some conditions. This is performed in the same way as the conjugation of VHHs.

Excess VHH, FITC-labelled VHH and Cys-PEG3-FITC dye that was not conjugated was removed from the LNP solutions by spin filtration. This is done 4 times with Amicon Ultra-0.5 spin filters at 14000 rpm for 10 minutes. For recovery of the LNPs, the spin filters were spun upside down for 2 minutes at 1000 rpm.

2.5 Dynamic Light Scattering (DLS)

DLS is performed with a ZetaSizer Nano S (Malvern) to determine the hydrodynamic size and the polydispersity index (PDI). DLS samples were made by diluting the LNP solutions 50x in PBS (pH 7.4) and pipetting them in Greiner bio one 613101 semi-microcuvets. The samples for zeta potential measurements were prepared the same way but were loaded into DTS1070 Zeta cells. All measurements were performed at 25 °C and a measurement angle of 173°. For every condition, three measurements of multiple runs were done with an equilibration time of 60s.

2.6 Scanning Electron Microscopy (SEM)

To observe the morphology of the formed LNPs, SEM was done. SEM samples were prepared by pipetting 20 µL of the solution of LNPs in MilliQ water on an SEM stub with carbon tape. After letting it dry overnight at room temperature, the samples were sputter-coated with gold using a Cressington Sputter Coater 108. The samples were then imaged using a JEOL JSM-IT100 Scanning Electron Microscope.

2.7 SDS-PAGE with Coomassie Blue staining

SDS-PAGE with Coomassie Blue staining is used to try to quantify whether the VHHs are conjugated to maleimide groups of the DSPE-PEG-Mal phospholipids on the LNP surface. SDS-PAGE samples were prepared by adding all sample conditions described above to a 4x loading buffer (β-mercaptoethanol 1:9 Laemmli sample buffer). The samples were then heated to 95 °C for 5 min and spinned down. The gel tank is filled with a 1x solution of the 1x SDS running buffer diluted with demi water. After loading the 4-15% Bio-Rad pre-cast gel in the tank, 20µL of all samples were loaded into the gel. Gel electrophoresis was performed at 100V for 20 min and 160V for 40 min. After electrophoresis, the gel was rinsed with MilliQ and placed in a tray with fixation buffer (50% methanol, 10% acetic acid, 40% demi water) overnight. Then the gel was stained by loading it in a tray with Coomassie stain (fixation buffer + 0,25% w/v Coomassie Blue R-250) and incubating the tray on a shaker for 2 hours at room temperature. Destaining was performed with a destaining solution (5% methanol, 7.5% acetic acid, 87.5% demi water) for 5 hours and refreshing the solution 4 times. After washing with MilliQ, the gel was imaged with a FluorChem M system from ProteinSimple.

2.7.1 Western blot with antibody probing

The Western blot is performed the same way as SDS-PAGE up until the electrophoresis. After electrophoresis, the gel was placed on a Trans-Blot transfer membrane and in the cassette of a Trans-Blot Turbo system from Bio-Rad. Then the Trans-Blot Turbo was run on the Turbo protocol. After running, the membranes were washed in 20 mL washing buffer (PBS-T) and transferred to a 50 mL tube containing 5 mL of blocking buffer (PBS-T, 5% BSA). In this tube were incubated for 45 minutes under constant mixing. Then antibody probing was done with an anti-VHH rabbit antibody. For antibody probing, the membrane is transferred to a new 50 mL tube containing 5 mL blocking buffer and an excess of anti-VHH rabbit antibody. This is then incubated overnight at 4 °C under constant stirring. The next day the membrane was washed 6x for 10 minutes in 20 mL washing buffer on a shaker. After washing, a second antibody probing was done transferring the membrane to a 50 mL tube containing 2.5 µL anti-rabbit-HRP (1:2.000 diluted), 0.5 µL StrepTactin-HRP-conjugate and 5 mL of washing buffer. This tube was incubated at room temperature for 1 hour and then washed 6x for 5 minutes. Imaging of the membrane was done with a FluorChem M system from ProteinSimple. HRP substrate Working Solution (50% Stable Peroxide solution, 50% Luminol/Enhancer Solution) is

used for anti by pipetting it on the membrane covering the whole surface. Fluorescent Cy5.5 images were also taken with the FluorChem M system on this membrane.

2.7.2 Measuring Cy5.5 and FITC fluorescence

Samples for measuring fluorescence were prepared in a 96-well plate by pipetting 50µL LNP solution and 50µL MilliQ in each well. Fluorescence on the plate was measured with a Varioskan LUX plate reader from ThermoFischer. The emission and excitation wavelengths in the software are set to that of Cy5.5 (492/517nm) and FITC (675/695nm).

2.7.3 LNP uptake by RAW 264.7 macrophages

LNP uptake by RAW 264.7 macrophages is analysed in two different ways; by an EVOS Fluorescence microscope and a Zeiss LSM880 Confocal microscope. For these different methods of imaging, the RAW macrophages were also seeded on different surfaces. Before preparing the samples, the RAW 264.7 macrophages were passaged to P16 in a T75 cell culture flask.

The RAW macrophages having a 90% confluence are harvested from the T75 flask using trypsin. The harvested cells were then seeded at 20.000 cells/cm^2 in both a 96-well plate and two Lab-Tek 8-well Chamber Slides. This was done in a culture medium (DMEM, 10% FBS and 1% Pen/Strep) and incubated overnight at 37 °C. After overnight incubation of the cells in the medium, the cells were incubated for 3 hours with 100 µL of LNP solution in MilliQ and 200 µL of cell culture medium per well.

After 3 hours of incubation of the macrophages with LNPs, the samples in the 96-well plate were washed 3 times with PBS and imaged with the EVOS Fluorescence microscope. The samples in the two Lab-Tek 8-well Chamber Slides were fixed by removing the medium from the cells. Then 1 mL of 4% (w/v) formaldehyde solution in PBS was added to the cells and this was incubated for 15 minutes. In addition, a DAPI staining was performed on all samples in the two Lab-Tek 8-well Chamber Slides. First, all conditions were washed 3 times with PBS. DAPI was added in a 100x dilution in PBS and added to the cells. After 10 minutes of incubation at room temperature, the DAPI dilution was removed and the cells were again washed 3 times with PBS. These samples were then imaged with the Zeiss LSM880 Confocal microscope.

3 Results

Many different LNPs and LNP-VHH conjugates were made; LNPs with and without DSPE-PEG-Mal are conjugated with different estimated amounts of VHHs per LNP. The LNPs are characterized, conjugation of VHH is quantified and LNP uptake by macrophages is observed.

3.1 LNP characterization

3.1.1 Dynamic Light Scattering (DLS)

DLS measurements were performed to determine the hydrodynamic size. The DLS results show the hydrodynamic size expressed in the diameter of LNPs. This is done on LNPs with or without DSPE-PEG-Mal and different estimated amounts of VHHs per LNP. The results are shown in Figure 4. The first measurement was performed on a batch that had 1, 10, and 10^2 VHHs per LNP and was not filtered. The second measurement was performed on a batch that had 10^3 and 10^5 VHHs per LNP. From both batches LNPs without VHHs were also measured.

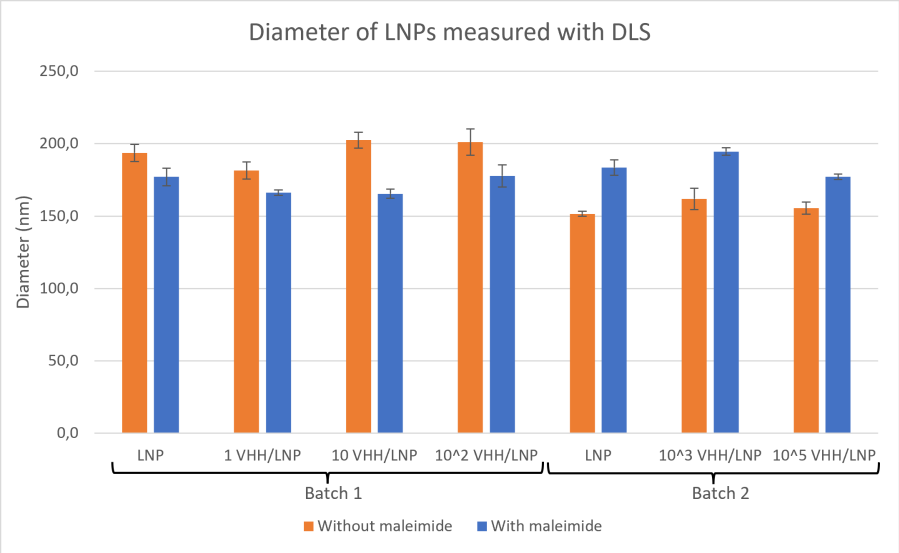

Figure 4: *DLS results of hydrodynamic size expressed in the diameter of LNPs with or without DSPE-PEG-Mal and different estimated amounts of VHHs conjugated per LNP.*

The DLS measurements show that the hydrodynamic size is around 180 nm. The results of the first batch of LNPs show that the LNPs with DSPE-PEG-Mal seem to be bigger in general. However, this is the other way around in the second batch. So, not much can be said about the influence of DSPE-PEG-Mal in the LNP composition or the amount of VHHs per LNP on the hydrodynamic size. Furthermore, the polydispersity is relatively high, indicating that the LNPs do vary in size. The polydispersity is shown in Table 7 as the PDI.

Table 7: *DLS results of the PDI, in which in each condition the first column is without DSPE-PEG-Mal and the second column is with DSPE-PEG-Mal in the LNP composition.*

Batch 1								**Batch 2**					
LNP		**1 VHH/LNP**		**10 VHH/LNP**		**10^2 VHH/LNP**		**LNP**		**10^3 VHH/LNP**		**10^5 VHH/LNP**	
0,320	0,378	0,155	0,248	0,172	0,293	0,170	0,251	0,251	0,337	0,287	0,310	0,236	0,221

Zeta potential measurements were performed on the same conditions as the DLS measurements. In addition, VHH and dsDNA only were measured. DLS results of zeta potential are shown in Figure 5.

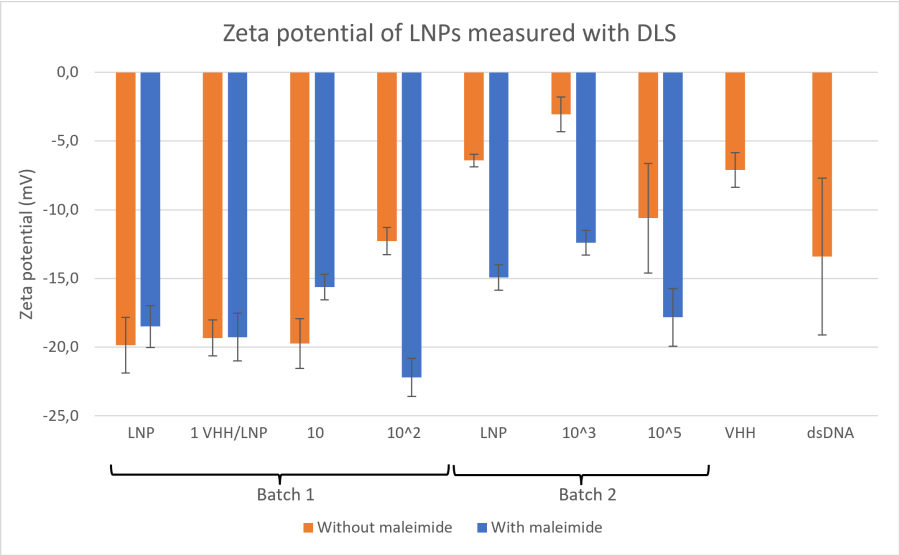

Figure 5: *Zeta potential results of the LNPs with or without DSPE-PEG-Mal and different estimated amounts of VHHs conjugated per LNP. Also, the zeta potential of VHHs and dsDNA only is shown.*

The LNPs without VHHs and with low amounts of VHHs per LNPs of the first batch have a surface charge of around -19 mV. In these results, one thing is really interesting because, at 10^2 VHHs per LNP, a significant difference is visible in surface charge between the LNPs with and without DSPE-PEG-Mal. This also seems to be the case in the second batch, however in this batch there also is a big difference in LNPs with and without DSPE-PEG-Mal, that don't have VHHs conjugated to them. Therefore, not much can be said about the influence of DSPE-PEG-Mal in the LNP composition and the conjugation of VHHs on the surface charge.

3.1.2 Scanning Electron Microscopy (SEM)

Scanning Electron Microscopy (SEM) is used to observe the morphology and structure of the formed LNPs. Two samples were made; LNPs without DSPE-PEG-Mal and LNPs with DSPE-PEG-Mal, they are shown in Figure 6.

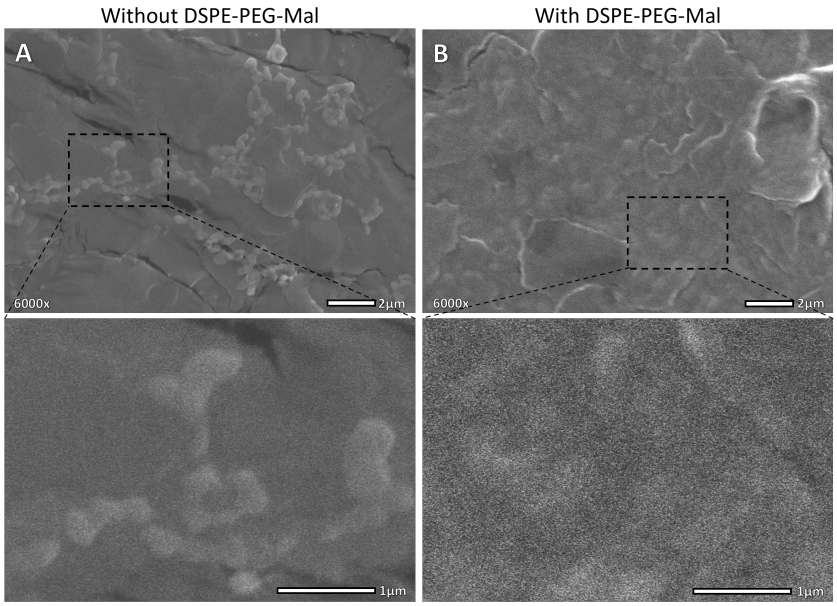

Figure 6: *SEM images of LNP samples 6000x magnified, with a crop of the visible LNPs below. (A) LNPs without DSPE-PEG-Mal. (B) LNPs with DSPE-PEG-Mal.*

In the SEM images groups of LNPs are visible, with in the cropped images below also individual LNPs visible. In the LNPs with DSPE-PEG-Mal, these individual LNPs are not as clearly visible as

compared to the LNPs without DSPE-PEG-Mal. This might be due to interactions with the carbon tape because the structures seem to be more attached to the surface. In addition, the quality of this image is somewhat lower. The overall morphology of LNPs is round but in these SEM images, they do sometimes interact with each other and form small clusters. The average LNP diameters are analyzed from these SEM images using ImageJ and are shown in Table 8.

Table 8: *Average LNP diameters determined from Figure 6 using ImageJ.*

	Average d. (nm)	**Std. dev.**
LNPs without DSPE-PEG-Mal	291,2	58,3
LNPs with DSPE-PEG-Mal	438,8	80,3

These diameters differ a lot from the hydrodynamic diameters determined by the DLS measurements in Figure 4. This can be explained by the fact that the hydrodynamic size with DLS is measured in a different way. Also, the SEM images are made of a different batch of LNPs than where DLS was performed on. Nevertheless, both LNP characterization experiments indicate that LNPs are formed, although there is a large variety in size.

3.2 Conjugation quantification

3.2.1 SDS-PAGE with Coomassie Blue staining

SDS-PAGE is used to quantify whether VHHs were conjugated to the LNPs containing maleimide groups on their surface. The SDS solution used in this method breaks the LNPs apart, after which only VHHs and VHH-lipid conjugates should run through the gel. This means that LNPs without VHHs should give no band on the gel. LNP samples without maleimide and with VHH would provide a band at the same height as VHH only, around 17.8 kDa. LNP samples with maleimide and with VHH would give a band at the height of DSPE-PEG-Mal-VHH conjugates, around 20.7 kDa.

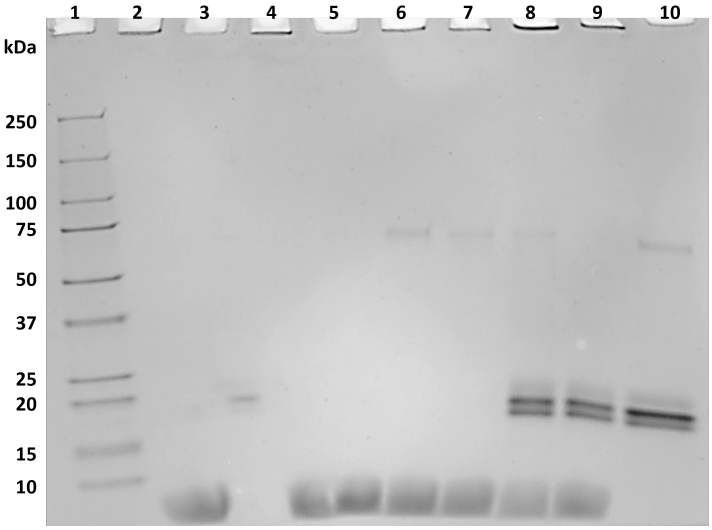

Lane	**Sample**
1	MW Ladder
2	LNP + Mal
3	-
4	10 VHHs/ LNP
5	10 VHHs/ LNP + Mal
6	10^3 VHHs/ LNP
7	10^3 VHHs/ LNP + Mal
8	10^5 VHHs/ LNP
9	10^5 VHHs/ LNP + Mal
10	VHHs

Figure 7: *Results of SDS-PAGE on samples of LNPs, VHHs and LNPs with and without DSPE-PEG-Mal that have different amounts of VHHs added to them.*

The results in Figure 7 show only clear bands at VHHs only (lane 10) and at 10^5 VHHs per LNP (lane 8-9). These bands appear around 17.8 kDa, which is the molecular weight of the VHHs. No bands are visible around 20.9 kDa at all LNP conditions with DSPE-PEG-Mal. This could mean that DSPE-PEG-Mal-VHH conjugates are absent or that SDS-PAGE is not sensitive enough to measure a low concentration of conjugates. Furthermore, light bands are visible around 70 kDa for 10^3 VHHs per LNP, 10^5 VHHs per LNP and VHHs only. A possible explanation could be that multiple VHHs cluster together forming a band at this molecular weight. This band is the lightest at 10^5 VHHs per LNP with DSPE-PEG-Mal, which could suggest that some of those VHHs actually did form conjugates with DSPE-PEG-Mal. Furthermore, the lipids in the running front of the gel are also stained and show clearly visible bands.

3.2.2 Western blot

Western Blotting is performed, because SDS-PAGE may not be sensitive enough to detect the VHH-lipid conjugates. This is conducted on a batch with 10^4 VHHs per LNP, because 10^5 VHHs per LNP shows large amounts of unconjugated VHHs in the SDS-PAGE, while 10^3 VHHs per LNP shows no VHHs at all. Furthermore, LNPs containing DSPE-PEG-N-Cy5.5, LNPs and having 10^4 FITC-labelled VHHs conjugated and LNPs having Cys-PEG3-FITC dye conjugated to them were also loaded into the gel for western blotting. Before loading into the gel the samples were all filtrated with spin filtration, except for the sample of LNPs containing DSPE-PEG-Mal and DSPE-PEG-N-Cy5.5 (lane 10). This sample is not filtered, because no VHHs or dye had to be removed. The western blot with antibody detection for VHHs is shown in Figure 8.

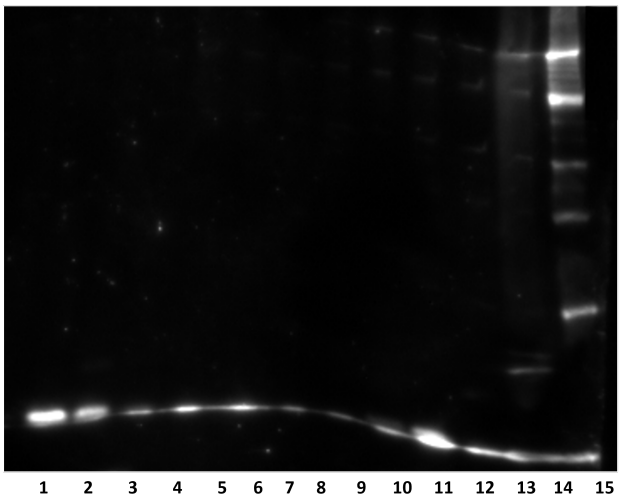

Lane	LNP type	Conjugated molecule
1	LNPs	VHH
2		VHH-FITC
3		FITC
4	Mal	VHH
5		VHH-FITC
6		FITC
7	Cy5.5	VHH
8		VHH-FITC
9		FITC
10	Mal Cy5.5	-
11		VHH
12		VHH-FITC
13		FITC
14	No LNPs	VHH only
15		Ladder

Figure 8: *Western blot on samples of LNPs with and without DSPE-PEG-Mal and DSPE-PEG-N-Cy5.5 having VHHs, FITC-labelled VHHs and Cys-PEG3-FITC dye conjugated to them*

In the western blot with antibody detection, the band around 17.8 kDa of VHHs (lane 14) is visible. Apart from some diffusion of the DNA ladder in the upper right corner, not much is visible on the rest of this membrane from the western blot. This may be caused by the loss of LNP-VHH conjugates due to spin filtration. In addition, the membrane for western blotting was used for measuring the fluorescence of Cy5.5 that is coming from DSPE-PEG-N-Cy5.5. This way the presence of this lipid in the LNP composition can be quantified because excess DSPE-PEG-N-Cy5.5 was removed by dialysis after LNP synthesis. The fluorescence of Cy5.5 on the membrane is shown in Figure 9.

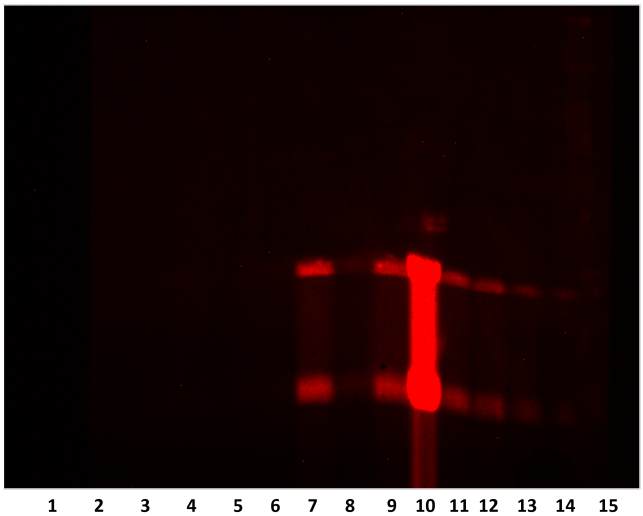

Lane	LNP type	Conjugated molecule
1	LNPs	VHH
2		VHH-FITC
3		FITC
4	Mal	VHH
5		VHH-FITC
6		FITC
7	Cy5.5	VHH
8		VHH-FITC
9		FITC
10	Mal Cy5.5	-
11		VHH
12		VHH-FITC
13		FITC
14	No LNPs	VHH only
15		Ladder

Figure 9: *Fluorescence of Cy5.5 on the membrane used for western blotting that has samples of LNPs with and without DSPE-PEG-Mal and DSPE-PEG-N-Cy5.5 having VHHs, FITC-labelled VHHs and Cys-PEG3-FITC dye conjugated to them.*

This Figure shows that Cy5.5 is strongly present in the unfiltered sample of LNPs containing DSPE-PEG-Mal and DSPE-PEG-N-Cy5.5 (lane 10). In most other samples with LNPs that have DSPE-PEG-N-Cy5.5 (lanes 7-13) fluorescence of Cy5.5 is also visible. Again, due to spin filtration, this signal is less intense than the unfiltered sample. Unfortunately, the molecular weight at which this fluorescence is located is unknown because the DNA ladder is not visible. However, this shows that DSPE-PEG-N-Cy5.5 is indeed present in the LNP composition. This suggests a high possibility of DSPE-PEG-Mal also being present in the LNP composition.

3.2.3 Measuring Cy5.5 and FITC fluorescence

To further quantify whether the DSPE-PEG-N-Cy5.5 is present in the LNPs and whether the FITC-labelled VHHs and Cys-PEG3-FITC dye are conjugated to DSPE-PEG-Mal on the LNP surface, fluorescence intensity was measured. This is done on a batch of LNPs that has 10^4 VHHs, FITC-labelled VHHs and Cys-PEG3-FITC dye per LNP conjugated. Also, fluorescence was measured on the filtrate of each LNP solution from spin filtration after the conjugation. The LNPs that didn't undergo conjugation were not filtered, so no fluorescence was measured on their filtrate.

	LNP solutions				Filtrates		
	Unfil.	VHH	VHH-FITC	Cys-FITC	VHH	VHH-FITC	Cys-FITC
LNP	-0,1	0,0	0,0	0,0	-0,1	0,0	-0,1
LNP+Mal	0,3	0,2	0,0	0,1	0,1	-0,1	-0,1
LNP+Cy5.5	45,9	1,6	0,0	1,7	-0,1	-0,1	
LNP+Mal+Cy5.5	43,4	-0,1	0,3	0,0	0,1	0,0	0,1

Table 9: *Fluorescence intensity at the emission wavelength of Cy5.5 (695nm) of the LNP solutions and the filtrate obtained from spin filtration. Cells were coloured green for intensity above 1,0.*

In Table 9 of the fluorescence intensity at the emission wavelength of Cy5.5 (695nm), it is clearly visible that the unfiltered LNPs with DSPE-PEG-N-Cy5.5 show a way higher fluorescence intensity than the filtered LNPs with DSPE-PEG-N-Cy5.5 that have VHHs and dye conjugated to them. That is again because of the loss of LNPs during spin filtration. However, from this Table, it seems that some LNP samples that had DSPE-PEG-N-Cy5.5 added to their lipid mixture do indeed contain DSPE-PEG-N-Cy5.5, which correlates to the Cy5.5 fluorescence on the western blot membrane. Because the filtrate from spin filtration doesn't show fluorescence intensity, no free DSPE-PEG-N-Cy5.5 lipids are present in the LNP solutions.

	LNP solutions				Filtrates		
	Unfil.	VHH	VHH-FITC	Cys-FITC	VHH	VHH-FITC	Cys-FITC
LNP	0,0	0,0	0,6	2,9	0,0	0,6	2,8
LNP+Mal	0,0	0,0	0,2	4,4	0,0	8,4	3,3
LNP+Cy5.5	0,2	0,0	0,1	1,4	0,0	4,1	
LNP+Mal+Cy5.5	0,1	0,1	0,0	0,5	0,0	5,6	4,3

Table 10: *Fluorescence intensity at the emission wavelength of FITC (517nm) of the LNP solutions and the filtrate obtained from spin filtration. Cells were coloured green for intensity above 1,0.*

In Table 10 of the fluorescence intensity at the emission wavelength of FITC (517nm) most fluorescence intensity is found in the filtrate of the LNPs conjugated with the FITC-labelled VHHs and Cys-PEG3-FITC dye. This shows that a large part of FITC-labelled VHHs and Cys-PEG3-FITC dye are not conjugated to the LNPs and are removed during spin filtration. The column of LNPs with Cys-PEG3-FITC dye shows high fluorescence intensity, either in LNPs with or without DSPE-PEG-Mal. This suggests that this dye attaches to all LNP types and not much can be said about specific conjugation with maleimide on the LNP surface. Unfortunately, the column of LNPs with FITC-labelled VHHs shows very little FITC fluorescence, suggesting not much is conjugated to the LNPs. This can be explained by the non-fouling nature of the PEG coating on the LNPs surface, which can make the conjugation of VHHs to the maleimide groups more difficult. The difference between FITC-labelled VHHs and the Cys-PEG3-FITC can be caused by the smaller size of the Cys-PEG3-FITC compared to the FITC-labelled VHHs, allowing for more space for conjugation.

3.3 LNP uptake by RAW macrophages

To see the uptake of the LNPs by macrophages, a cell experiment with the RAW 264.7 macrophage cell line is performed. This is done on a batch of LNPs containing DSPE-PEG-N-Cy5.5. These LNPs have nothing conjugated or have 10^4 VHHs, FITC-labelled VHHs or Cys-PEG3-FITC dye per LNP conjugated. The uptake of LNPs is imaged with two microscopes: an EVOS Fluorescence microscope and a Zeiss LSM880 Confocal microscope.

3.3.1 EVOS Fluorescence microscope

As controls, a blank condition with only macrophages and a condition of free VHH-FITC added to the macrophages were taken into account, shown in Figure 10.

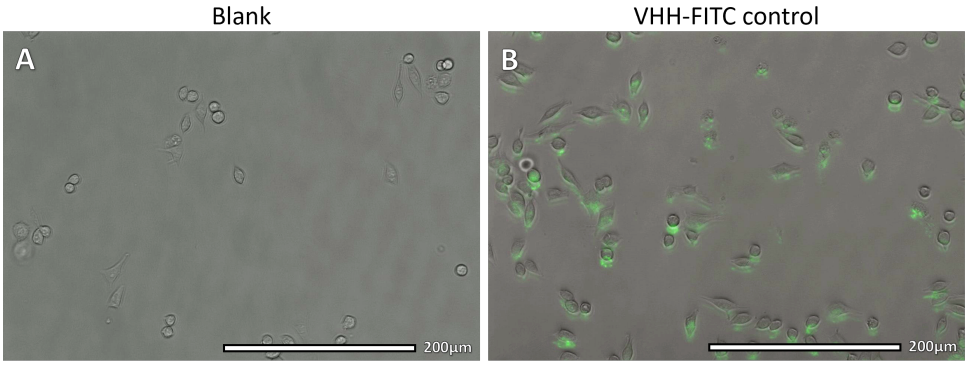

Figure 10: *EVOS microscopic images of controls with macrophages. (A) Blank condition containing macrophages only. (B) Condition containing macrophages with free VHH-FITC added.*

The blank condition shows the macrophages without fluorescence because no dyes were present. The other control containing free VHH-FITC shows that the macrophages take up these FITC-labelled VHHs. Figure 11 shows the other conditions revealing some fluorescence.

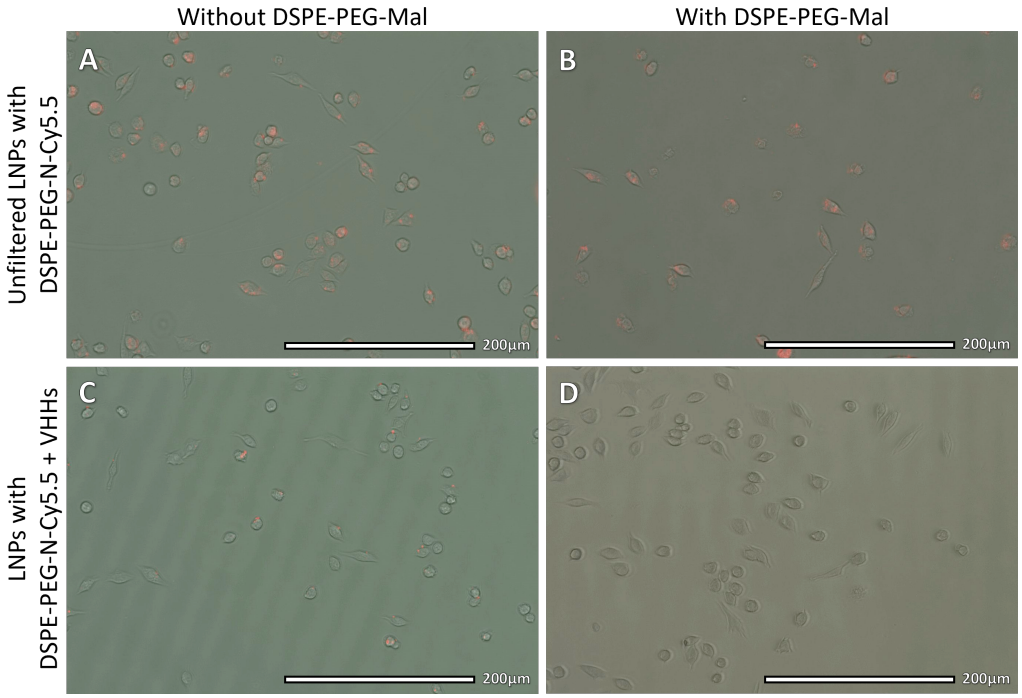

Figure 11: *EVOS microscopic images of the conditions showing the most fluorescence that contain LNP added to the macrophages. Unfiltered LNPs containing DSPE-PEG-N-Cy5.5 (A) without DSPE-PEG-Mal and (B) with DSPE-PEG-Mal. Filtered LNPs containing DSPE-PEG-N-Cy5.5 and VHHs (C) without DSPE-PEG-Mal and (D) with DSPE-PEG-Mal.*

In these images only the fluorescence of Cy5.5 is visible, especially in the unfiltered LNPs with DSPE-PEG-N-Cy5.5 without anything conjugated. Another condition showing some fluorescence of Cy5.5 is LNPs with DSPE-PEG-N-Cy5.5, without DSPE-PEG-Mal and having VHHs conjugated to them. The same as in the western blot and measuring fluorescence, the spin filtration caused a lot of LNPs to be removed. This is probably why no fluorescence is visible in the other filtered conditions. Without this loss of fluorescent LNPs, something could have been said about the difference in the number of LNPs taken up by the macrophages. However, this was not possible due to the significant difference in the number of LNPs that was present between all LNP solutions after spin filtration.

3.3.2 Zeiss LSM880 Confocal microscope

Again as controls, a blank condition with only macrophages and a condition of free VHH-FITC added to the macrophages were taken into account, shown in Figure 12.

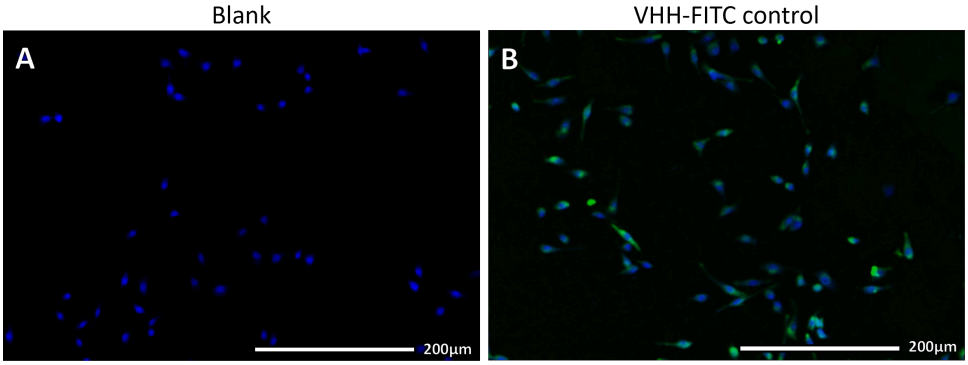

Figure 12: *Zeiss LSM880 Confocal microscopic images of controls with macrophages. (A) Blank condition containing macrophages only. (B) Condition containing macrophages with free VHH-FITC added.*

These control conditions analysed with the confocal microscope show the same as the control of the fluorescence microscope in Figure 10. Only DAPI is present in the blank condition showing the macrophage nuclei. The VHH-FITC control shows that free VHH-FITC is taken up by the macrophages. The other conditions displaying some fluorescence are shown in Figure 13.

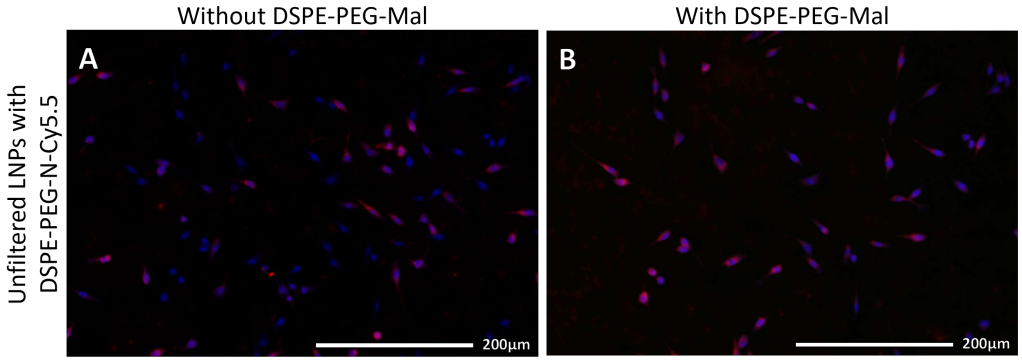

Figure 13: *Zeiss LSM880 Confocal microscopic images of the conditions showing the most fluorescence that contain LNP added to the macrophages. Unfiltered LNPs containing DSPE-PEG-N-Cy5.5 (A) without DSPE-PEG-Mal and (B) with DSPE-PEG-Mal.*

The same as in the images of the EVOS fluorescence microscope of Figure 11, the unfiltered LNPs with DSPE-PEG-N-Cy5.5 without anything conjugated showed most fluorescence of Cy5.5. All filtered LNP conditions showed no Cy5.5 or FITC fluorescence, probably again due to spin filtration. Although this loss of LNPs, unfiltered LNP conditions do show that LNPs are taken up by RAW 264.7 macrophages.

4 Discussion

In the synthesis of the LNPs, the T-tube method was used. This method is a less accurate way of making the LNPs because this process is not well automated and doesn't make use of a microfluidic mixing chip. This causes the LNPs in this study to be more polydisperse with a PDI of around 0,3. Studies using an automated device like the NanoAssemblr reported PDIs of around 0,1 or even lower [79, 80]. This relatively high polydispersity should not have a big effect on the VHH conjugation but can have an effect on LNP uptake by macrophages. Also, this could have been an explanation for the difference in zeta potential between LNP batches and solutions.

Furthermore, the use of dsDNA and tRNA caused the LNP batches to have different properties. While there was tried to minimize the differences in LNP synthesis between these two nucleic acids, this was unavoidable. DLS measurements and the SDS-PAGE were performed with batches of LNPs containing dsDNA, while the rest of the experiments were performed with LNPs containing tRNA. Experiments on LNPs containing different nucleic acids were therefore not compared. Also eventually, miRNA should be used for targeting macrophages with LNPs and the synthesis would need to be optimised for this.

After conjugation of the VHHs, most of the batch with tRNA-loaded LNPs was filtered using spin filtration. This was done to remove unconjugated VHHs and Cys-PEG3-FITC dye. During this spin filtration, most LNPs got stuck to the filter and weren't recovered in the LNP solutions. This caused that unfiltered and filtered conditions couldn't be compared. But most importantly it caused that the results of the western blot, fluorescence measurements and LNP uptake experiment could not be interpreted as they should. Because of the low concentration of LNPs left, the western blot did not show any VHHs in LNP solutions, fluorescence measurements showed significantly lower intensity than in unfiltered conditions and almost no LNP uptake is observed in the uptake experiment. Therefore from these experiments, not many conclusions can be drawn about maleimide reactivity on the LNP surface, VHH conjugation to LNPs and LNP uptake of different LNP conditions. An alternative for spin filtration to remove unconjugated VHHs and dyes would be dialysis. This should be done with a filtration membrane with a pore size of around 40 kDa MWCO or bigger so that any VHH dimers are also filtered out.

Alternatively, the conjugation of VHHs to LNPs could have been done with other methods. In these methods VHHs are first conjugated to free DSPE-PEG-Mal lipids, to form lipid-VHH conjugates. By first forming these lipid-VHH conjugates, the binding characteristics can be tested. LNP synthesis with the lipid-VHH conjugates can be done by adding them to the lipid mixture, after which the LNPs can be formed with the T-tube method. Another way is by first forming LNPs without the lipid-VHH conjugates and adding them to the LNP solution after which post-insertion takes place [81].

The optimal VHH concentration that needs to be added to an LNP solution is unknown. In addition, the DSPE-PEG-Mal concentration in the lipid mixture optimal for this conjugation is also unknown. The efficiency of VHH conjugation to a lipid surface containing DSPE-PEG-Mal is something that needs to be optimized, before trying to target macrophages with such a LNP system. If the system of LNPs containing DSPE-PEG-Mal for conjugation of VHH doesn't work, alternatives from Section 1.5 can be used. An example is conjugation with click chemistry, by using DSPE-PEG-DBCO in the lipid mixture that conjugates to azides attached to the VHHs via a linker [81].

Lastly, this report should be considered as a proof of concept to show whether DSPE-PEG-Mal is reactive for conjugation on the surface of LNPs loaded with nucleic acids. The TNFα-specific VHHs don't target macrophages, so this system is not able to show uptake of LNPs with macrophage-specific VHHs. Also, the nucleic acids used are not able to influence the behaviour of macrophages, while miRNA is able to do that.

5 Conclusion

In this report, the formation of LNPs having VHHs conjugation was studied. As expected, ionizable LNPs containing dsDNA or tRNA were formed using the T-tube method. Conjugation of VHHs via maleimide-thiol chemistry should be possible by using phospholipid DSPE-PEG-Mal in the lipid mixture. However, this conjugation is not observed in experiments which may be caused by DSPE-PEG-Mal not being reactive or available on the LNP surface for VHH conjugation. This can be changed by optimizing the concentration of DSPE-PEG-Mal in the lipid mixture and the concentration of VHHs during conjugation. While conjugation is not yet established, LNPs are taken up by macrophages.

In conclusion, the proof of concept used in this study doesn't yet deliver a promising outcome to start testing with macrophage-specific VHHs and doing extensive testing with macrophages.

Acknowledgements

First, I want to thank everybody at the Developmental BioEngineering group for making me feel welcome and helping me out. Of course, I am grateful for being able to have made use of their labs and material.

I want to thank Prof. dr. Marcel Karperien for helping me during my assignment and giving me feedback on my bachelor's assignment.

Furthermore, I want to thank dr. Bram Zoetebier and dr. Jan Hendriks for being my daily supervisors, guiding me through this bachelor's assignment and giving me feedback.

Lastly, I would like to thank dr. Ruchi Bansal for being an extern member of the examination commission and giving me some experiment material.

References

[1] Sanchez-Lopez E, Coras R, Torres A, Lane NE, Guma M. Synovial inflammation in osteoarthritis progression. Nat Rev Rheumatol. 2022 May;18:258-75. doi:10.1038/s41584-022-00749-9.

[2] Musumeci G, Aiello FC, Szychlinska MA, Di Rosa M, Castrogiovanni P, Mobasheri A. Osteoarthritis in the XXIst century: risk factors and behaviours that influence disease onset and progression. Int J Mol Sci. 2015 Mar;16(3):6093-112. doi:10.3390/ijms16036093.

[3] Chen Y, Jiang W, Yong H, He M, Yang Y, Deng Z, et al. Macrophages in osteoarthritis: pathophysiology and therapeutics. Am J Transl Res. 2020 Jan;12(1):261-8. Available from: https://pubmed.ncbi.nlm.nih.gov/32051751.

[4] Zhang H, Cai D, Bai X. Macrophages regulate the progression of osteoarthritis. Osteoarthritis Cartilage. 2020 May;28(5):555-61. doi:10.1016/j.joca.2020.01.007.

[5] Mushenkova NV, Nikiforov NG, Shakhpazyan NK, Orekhova VA, Sadykhov NK, Orekhov AN. Phenotype Diversity of Macrophages in Osteoarthritis: Implications for Development of Macrophage Modulating Therapies. Int J Mol Sci. 2022 Aug;23(15). doi:10.3390/ijms23158381.

[6] Kapellos TS, Bonaguro L, Gemünd I, Reusch N, Saglam A, Hinkley ER, et al. Human Monocyte Subsets and Phenotypes in Major Chronic Inflammatory Diseases. Front Immunol. 2019 Aug;10:2035. doi:10.3389/fimmu.2019.02035.

[7] Cormican S, Griffin MD. Human Monocyte Subset Distinctions and Function: Insights From Gene Expression Analysis. Front Immunol. 2020 Jun;11:1070. doi:10.3389/fimmu.2020.01070.

[8] Cros J, Cagnard N, Woollard K, Patey N, Zhang SY, Senechal B, et al. Human CD14dim Monocytes Patrol and Sense Nucleic Acids and Viruses via TLR7 and TLR8 Receptors. Immunity. 2010 Sep;33(3):375-86. doi:10.1016/j.immuni.2010.08.012.

[9] Wong KL, Tai JJY, Wong WC, Han H, Sem X, Yeap WH, et al. Gene expression profiling reveals the defining features of the classical, intermediate, and nonclassical human monocyte subsets. Blood. 2011 Aug;118(5):16-31. doi:10.1182/blood-2010-12-326355.

[10] Zawada AM, Rogacev KS, Rotter B, Winter P, Marell RR, Fliser D, et al. SuperSAGE evidence for CD14++CD16+ monocytes as a third monocyte subset. Blood. 2011 Sep;118(12):50-61. doi:10.1182/blood-2011-01-326827.

[11] Moreno-Fierros L, García-Hernández AL, Ilhuicatzi-Alvarado D, Rivera-Santiago L, Torres-Martínez M, Rubio-Infante N, et al. Cry1Ac protoxin from Bacillus thuringiensis promotes macrophage activation by upregulating CD80 and CD86 and by inducing IL-6, MCP-1 and TNF-α cytokines. Int Immunopharmacol. 2013 Dec;17(4):1051-66. doi:10.1016/j.intimp.2013.10.005.

[12] Cutolo M, Campitiello R, Gotelli E, Soldano S. The Role of M1/M2 Macrophage Polarization in Rheumatoid Arthritis Synovitis. Front Immunol. 2022;13. doi:10.3389/fimmu.2022.867260.

[13] Bertani FR, Mozetic P, Fioramonti M, Iuliani M, Ribelli G, Pantano F, et al. Classification of M1/M2-polarized human macrophages by label-free hyperspectral reflectance confocal microscopy and multivariate analysis. Sci Rep. 2017;7. doi:10.1038/s41598-017-08121-8.

[14] Yao Y, Xu XH, Jin L. Macrophage Polarization in Physiological and Pathological Pregnancy. Front Immunol. 2019;10:792. doi:10.3389/fimmu.2019.00792.

[15] Lech M, Anders HJ. Macrophages and fibrosis: How resident and infiltrating mononuclear phagocytes orchestrate all phases of tissue injury and repair. Biochimica et Biophysica Acta (BBA) - Molecular Basis of Disease. 2013 Jul;1832(7):989-97. doi:10.1016/j.bbadis.2012.12.001.

[16] Self-Fordham JB, Naqvi AR, Uttamani JR, Kulkarni V, Nares S. MicroRNA: Dynamic Regulators of Macrophage Polarization and Plasticity. Front Immunol. 2017 Aug;8:1062. doi:10.3389/fimmu.2017.01062.

[17] Essandoh K, Li Y, Huo J, Fan GC. MiRNA-Mediated Macrophage Polarization and its Potential Role in the Regulation of Inflammatory Response. Shock. 2016 Aug;46(2):122-31. doi:10.1097/SHK.0000000000000604.

[18] Zhang Y, Zhang M, Zhong M, Suo Q, Lv K. Expression profiles of miRNAs in polarized macrophages. Int J Mol Med. 2013 Apr;31(4):797-802. doi:10.3892/ijmm.2013.1260.

[19] Jiménez VC, Bradley EJ, Willemsen AM, van Kampen AHC, Baas F, Kootstra NA. Next-generation sequencing of microRNAs uncovers expression signatures in polarized macrophages. Physiol Genomics. 2014 Feb;46(3):91-103. doi:10.1152/physiolgenomics.00140.2013.

[20] Wang Z, Brandt S, Medeiros A, Wang S, Wu H, Dent A, et al. MicroRNA 21 Is a Homeostatic Regulator of Macrophage Polarization and Prevents Prostaglandin E2-Mediated M2 Generation. PLoS One. 2015 Feb;10(2):e0115855. doi:10.1371/journal.pone.0115855.

[21] Thulin P, Wei T, Werngren O, Cheung L, Fisher RM, Grandér D, et al. MicroRNA-9 regulates the expression of peroxisome proliferator-activated receptor δ in human monocytes during the inflammatory response. Int J Mol Med. 2013 May;31(5):1003-10. doi:10.3892/ijmm.2013.1311.

[22] Ying H, Kang Y, Zhang H, Zhao D, Xia J, Lu Z, et al. MiR-127 modulates macrophage polarization and promotes lung inflammation and injury by activating the JNK pathway. J Immunol. 2015 Feb;194(3):1239-51. doi:10.4049/jimmunol.1402088.

[23] O'Connell RM, Taganov KD, Boldin MP, Cheng G, Baltimore D. MicroRNA-155 is induced during the macrophage inflammatory response. Proc Natl Acad Sci USA. 2007 Jan;104(5):1604-9. doi:10.1073/pnas.0610731104.

[24] Chaudhuri AA, So AYL, Sinha N, Gibson WSJ, Taganov KD, O'Connell RM, et al. MiR-125b potentiates macrophage activation. Journal of immunology (Baltimore, Md : 1950). 2011 Nov;187(10):5062-8. doi:10.4049/jimmunol.1102001.

[25] Caescu CI, Guo X, Tesfa L, Bhagat TD, Verma A, Zheng D, et al. Colony stimulating factor-1 receptor signaling networks inhibit mouse macrophage inflammatory responses by induction of microRNA-21. Blood. 2015 Feb;125(8):1-13. doi:10.1182/blood-2014-10-608000.

[26] Sun Y, Li Q, Gui H, Xu DP, Yang YL, Su DF, et al. MicroRNA-124 mediates the cholinergic anti-inflammatory action through inhibiting the production of pro-inflammatory cytokines. Cell Res. 2013 Nov;23(11):1270-83. doi:10.1038/cr.2013.116.

[27] Chen Q, Wang H, Liu Y, Song Y, Lai L, Han Q, et al. Inducible MicroRNA-223 Down-Regulation Promotes TLR-Triggered IL-6 and IL-1β Production in Macrophages by Targeting STAT3. PLoS One. 2012;7(8):e42971. doi:10.1371/journal.pone.0042971.

[28] Jiang P, Liu R, Zheng Y, Liu X, Chang L, Xiong S, et al. MiR-34a inhibits lipopolysaccharide-induced inflammatory response through targeting Notch1 in murine macrophages. Exp Cell Res. 2012 Jun;318(10):1175-84. doi:10.1016/j.yexcr.2012.03.018.

[29] Zhang W, Liu H, Liu W, Liu Y, Xu J. Polycomb-mediated loss of microRNA let-7c determines inflammatory macrophage polarization via PAK1-dependent NF-κB pathway. Cell Death Differ. 2015 Feb;22(2):287-97. doi:10.1038/cdd.2014.142.

[30] Banerjee S, Xie N, Cui H, Tan Z, Yang S, Icyuz M, et al. MicroRNA let-7c regulates macrophage polarization. Journal of immunology (Baltimore, Md : 1950). 2013 Jun;190(12):6542-9. doi:10.4049/jimmunol.1202496.

[31] Liu F, Li Y, Jiang R, Nie C, Zeng Z, Zhao N, et al. miR-132 inhibits lipopolysaccharide-induced inflammation in alveolar macrophages by the cholinergic anti-inflammatory pathway. Exp Lung Res. 2015 Jun;41(5):261-9. doi:10.3109/01902148.2015.1004206.

[32] Taganov KD, Boldin MP, Chang KJ, Baltimore D. NF-κB-dependent induction of microRNA miR-146, an inhibitor targeted to signaling proteins of innate immune responses. Proc Natl Acad Sci USA. 2006 Aug;103(33):12481-6. doi:10.1073/pnas.0605298103.

[33] Banerjee S, Cui H, Xie N, Tan Z, Yang S, Icyuz M, et al. miR-125a-5p Regulates Differential Activation of Macrophages and Inflammation. J Biol Chem. 2013 Dec;288(49):35428-36. doi:10.1074/jbc.M112.426866.

[34] Ying W, Tseng A, Chang RCA, Morin A, Brehm T, Triff K, et al. MicroRNA-223 is a crucial mediator of PPARγ-regulated alternative macrophage activation. J Clin Invest. 2015 Nov;125(11):4149-59. doi:10.1172/JCI81656.

[35] Karunakaran D, Richards L, Geoffrion M, Barrette D, Gotfrit RJ, Harper ME, et al. Therapeutic Inhibition of miR-33 Promotes Fatty Acid Oxidation but Does Not Ameliorate Metabolic Dysfunction in Diet-Induced Obesity. Arterioscler, Thromb, Vasc Biol. 2015 Dec;35(12):2536-43. doi:10.1161/ATVBAHA.115.306404.

[36] Moore CS, Rao VTS, Durafourt BA, Bedell BJ, Ludwin SK, Bar-Or A, et al. miR-155 as a multiple sclerosis-relevant regulator of myeloid cell polarization. Ann Neurol. 2013 Nov;74(5):709-20. doi:10.1002/ana.23967.

[37] Ponomarev ED, Veremeyko T, Barteneva N, Krichevsky AM, Weiner HL. MicroRNA-124 promotes microglia quiescence and suppresses EAE by deactivating macrophages via the C/EBP-α-PU.1 pathway. Nat Med. 2011 Jan;17(1):64-70. doi:10.1038/nm.2266.

[38] Zhang S, Cheng Z, Wang Y, Han T. The Risks of miRNA Therapeutics: In a Drug Target Perspective. DDDT. 2021 Feb;15:721-33. doi:10.2147/DDDT.S288859.

[39] Fahmy TM, Fong PM, Goyal A, Saltzman WM. Targeted for drug delivery. Mater Today. 2005 Aug;8(8 Supplement):18-26. doi:10.1016/S1369-7021(05)71033-6.

[40] Patra JK, Das G, Fraceto LF, Campos EVR, Rodriguez-Torres MdP, Acosta-Torres LS, et al. Nano based drug delivery systems: recent developments and future prospects. J Nanobiotechnol. 2018 Dec;16(1):1-33. doi:10.1186/s12951-018-0392-8.

[41] Xu L, Wang X, Liu Y, Yang G, Falconer RJ, Zhao CX. Lipid Nanoparticles for Drug Delivery. Adv NanoBiomed Res. 2022 Feb;2(2):2100109. doi:10.1002/anbr.202100109.

[42] Battaglia L, Gallarate M. Lipid nanoparticles: state of the art, new preparation methods and challenges in drug delivery. Expert Opin Drug Deliv. 2012 May;9(5):497-508. doi:10.1517/17425247.2012.673278.

[43] Bulbake U, Doppalapudi S, Kommineni N, Khan W. Liposomal Formulations in Clinical Use: An Updated Review. Pharmaceutics. 2017 Jun;9(2):12. doi:10.3390/pharmaceutics9020012.

[44] Bozzuto G, Molinari A. Liposomes as nanomedical devices. Int J Nanomed. 2015 Feb;10:975-99. doi:10.2147/IJN.S68861.

[45] Dolatabadi JEN, Valizadeh H, Hamishehkar H. Solid Lipid Nanoparticles as Efficient Drug and Gene Delivery Systems: Recent Breakthroughs. Advanced Pharmaceutical Bulletin. 2015 Jun;5(2):151-9. doi:10.15171/apb.2015.022.

[46] Madkhali OA. Perspectives and Prospective on Solid Lipid Nanoparticles as Drug Delivery Systems. Molecules. 2022 Feb;27(5):1543. doi:10.3390/molecules27051543.

[47] Chauhan I, Yasir M, Verma M, Singh AP. Nanostructured Lipid Carriers: A Groundbreaking Approach for Transdermal Drug Delivery. Advanced Pharmaceutical Bulletin. 2020 Jun;10(2):150-65. doi:10.34172/apb.2020.021.

[48] Banerjee S, Kundu A. Lipid-drug conjugates: a potential nanocarrier system for oral drug delivery applications. DARU J Pharm Sci. 2018 Sep;26(1):65-75. doi:10.1007/s40199-018-0209-1.

[49] Irby D, Du C, Li F. Lipid–Drug Conjugate for Enhancing Drug Delivery. Mol Pharmaceutics. 2017 May;14(5):1325-38. doi:10.1021/acs.molpharmaceut.6b01027.

[50] Yoo J, Park C, Yi G, Lee D, Koo H. Active Targeting Strategies Using Biological Ligands for Nanoparticle Drug Delivery Systems. Cancers. 2019 May;11(5):640. doi:10.3390/cancers11050640.

[51] van Hensbergen Y, Broxterman HJ, Elderkamp YW, Lankelma J, Beers JCC, Heijn M, et al. A doxorubicin–CNGRC-peptide conjugate with prodrug properties. Biochem Pharmacol. 2002 Mar;63(5):897-908. doi:10.1016/S0006-2952(01)00928-5.

[52] Safavy A, Raisch KP, Khazaeli MB, Buchsbaum DJ, Bonner JA. Paclitaxel derivatives for targeted therapy of cancer: Toward the development of smart taxanes. J Med Chem. 2023;42(23):4919-24. doi:10.1021/jm990355x.

[53] Sable R, Jaynes J, Ronzetti M, Guzman W, Knotts Z, Val Nd, et al. Abstract B49: Precision targeting of M2-like macrophages by the innate defense regulator RP-182 in pancreatic cancer and noncancerous diseases. Cancer Res. 2019 Dec;79(24 Supplement):B49. doi:10.1158/1538-7445.PANCA19-B49.

[54] Mousavizadeh A, Jabbari A, Akrami M, Bardania H. Cell targeting peptides as smart ligands for targeting of therapeutic or diagnostic agents: a systematic review. Colloids Surf, B. 2017 Oct;158:507-17. doi:10.1016/j.colsurfb.2017.07.012.

[55] Yadav N, Francis AP, Priya VV, Patil S, Rajagopalan R. Polysaccharide-Drug Conjugates: A Tool for Enhanced Cancer Therapy. Polymers. 2022 Feb;14(5):950. doi:10.3390/polym14050950.

[56] Zhu G, Chen X. Aptamer-based targeted therapy. Adv Drug Delivery Rev. 2018 Sep;134:65-78. doi:10.1016/j.addr.2018.08.005.

[57] Cerchia L, Giangrande PH, McNamara JO, de Franciscis V. Cell-Specific Aptamers for Targeted Therapies. Methods in molecular biology (Clifton, NJ). 2009;535:59-78. doi:10.1007/978-1-59745-557-2_5.

[58] Mi J, Zhang X, Giangrande PH, McNamara JO, Nimjee SM, Sarraf-Yazdi S, et al. Targeted inhibition of $\alpha v\beta 3$ integrin with an RNA aptamer impairs endothelial cell growth and survival. Biochem Biophys Res Commun. 2005 Dec;338(2):956-63. doi:10.1016/j.bbrc.2005.10.043.

[59] Gragoudas ES, Adamis AP, Cunningham ET Jr, Feinsod M, Guyer DR. Pegaptanib for neovascular age-related macular degeneration. N Engl J Med. 2023;351(27):2805-16. doi:10.1056/NEJMoa042760.

[60] Kruspe S, Meyer C, Hahn U. Chlorin e6 Conjugated Interleukin-6 Receptor Aptamers Selectively Kill Target Cells Upon Irradiation. Mol Ther Nucleic Acids. 2014 Jan;3:e143. doi:10.1038/mtna.2013.70.

[61] Sylvestre M, Saxby CP, Kacherovsky N, Gustafson H, Salipante SJ, Pun SH. Identification of a DNA Aptamer That Binds to Human Monocytes and Macrophages. Bioconjugate Chem. 2020 Aug;31(8):1899-907. doi:10.1021/acs.bioconjchem.0c00247.

[62] Richards DA, Maruani A, Chudasama V. Antibody fragments as nanoparticle targeting ligands: a step in the right direction. Chem Sci. 2016 Dec;8(1):63-77. doi:10.1039/C6SC02403C.

[63] Harmsen MM, De Haard HJ. Properties, production, and applications of camelid single-domain antibody fragments. Appl Microbiol Biotechnol. 2007 Nov;77(1):13-22. doi:10.1007/s00253-007-1142-2.

[64] Kozani PS, Kozani PS, Rahbarizadeh F. The Potential Applicability of Single-Domain Antibodies (VHH): From Checkpoint Blockade to Infectious Disease Therapy. Trends in Med Sci. 2021 May;1(2). doi:10.5812/tms.114888.

[65] Liu M, Fang X, Yang Y, Wang C. Peptide-Enabled Targeted Delivery Systems for Therapeutic Applications. Front Bioeng Biotechnol. 2021 Jul;9:701504. doi:10.3389/fbioe.2021.701504.

[66] Lin X, Beringhs AO, Lu X. Applications of Nanoparticle-Antibody Conjugates in Immunoassays and Tumor Imaging. AAPS J. 2021 Mar;23(2):1-16. doi:10.1208/s12248-021-00561-5.

[67] Jazayeri MH, Amani H, Pourfatollah AA, Pazoki-Toroudi H, Sedighimoghaddam B. Various methods of gold nanoparticles (GNPs) conjugation to antibodies. Sens Bio-Sens Res. 2016 Jul;9:17-22. doi:10.1016/j.sbsr.2016.04.002.

[68] Saallah S, Lenggoro IW. Nanoparticles Carrying Biological Molecules: Recent Advances and Applications. Kona Powder Part J. 2018;35:89-111. doi:10.14356/kona.2018015.

[69] Boehnke N, Dolph KJ, Juarez VM, Lanoha JM, Hammond PT. Electrostatic Conjugation of Nanoparticle Surfaces with Functional Peptide Motifs. Bioconjugate Chem. 2020 Sep;31(9):2211-9. doi:10.1021/acs.bioconjchem.0c00384.

[70] Di Marco M, Shamsuddin S, Razak KA, Aziz AA, Devaux C, Borghi E, et al. Overview of the main methods used to combine proteins with nanosystems: absorption, bioconjugation, and encapsulation. Int J Nanomed. 2010;5:37-49.

[71] Spicer CD, Pashuck ET, Stevens MM. Achieving Controlled Biomolecule–Biomaterial Conjugation. Chem Rev. 2018 Aug;118(16):7702-43. doi:10.1021/acs.chemrev.8b00253.

[72] Hein CD, Liu XM, Wang D. Click Chemistry, A Powerful Tool for Pharmaceutical Sciences. Pharm Res. 2008 Oct;25(10):2216-30. doi:10.1007/s11095-008-9616-1.

[73] Lallana E, Sousa-Herves A, Fernandez-Trillo F, Riguera R, Fernandez-Megia E. Click Chemistry for Drug Delivery Nanosystems. Pharm Res. 2012 Jan;29(1):1-34. doi:10.1007/s11095-011-0568-5.

[74] Kolb HC, Sharpless KB. The growing impact of click chemistry on drug discovery. Drug Discovery Today. 2003 Dec;8(24):1128-37. doi:10.1016/S1359-6446(03)02933-7.

[75] Li H, Aneja R, Chaiken I. Click Chemistry in Peptide-Based Drug Design. Molecules. 2013 Aug;18(8):9797-817. doi:10.3390/molecules18089797.

[76] Żak MM, Zangi L. Lipid Nanoparticles for Organ-Specific mRNA Therapeutic Delivery. Pharmaceutics. 2021 Oct;13(10):1675. doi:10.3390/pharmaceutics13101675.

[77] Eygeris Y, Gupta M, Kim J, Sahay G. Chemistry of Lipid Nanoparticles for RNA Delivery. Acc Chem Res. 2022 Jan;55(1):2-12. doi:10.1021/acs.accounts.1c00544.

[78] Tam YYC, Chen S, Cullis PR. Advances in Lipid Nanoparticles for siRNA Delivery. Pharmaceutics. 2013 Sep;5(3):498-507. doi:10.3390/pharmaceutics5030498.

[79] Algarni A, Pilkington EH, Suys EJA, Al-Wassiti H, Pouton CW, Truong NP. In vivo delivery of plasmid DNA by lipid nanoparticles: the influence of ionizable cationic lipids on organ-selective gene expression. Biomater Sci. 2022 May;10(11):2940-52. doi:10.1039/D2BM00168C.

[80] Maeki M, Uno S, Niwa A, Okada Y, Tokeshi M. Microfluidic technologies and devices for lipid nanoparticle-based RNA delivery. J Controlled Release. 2022 Apr;344:80-96. doi:10.1016/j.jconrel.2022.02.017.

[81] Swart LE, Koekman CA, Seinen CW, Issa H, Rasouli M, Schiffelers RM, et al. A robust post-insertion method for the preparation of targeted siRNA LNPs. Int J Pharm. 2022 May;620:121741. doi:10.1016/j.ijpharm.2022.121741.